A deeply conserved protease, acylamino acid-releasing enzyme (AARE), acts in plant ageing

Sebastian N.W. Hoernstein[1], Buğra Özdemir[1*], Nico van Gessel[1], Alessandra A. Miniera[1], Bruno Rogalla von Bieberstein[1**], Lars Nilges[1], Joana Schweikert Farinha[1***], Ramona Komoll[1****], Stella Glauz[1], Tim Weckerle[1*****], Friedrich Scherzinger[1******], Marta Rodriguez-Franco[2], Stefanie J. Müller-Schüssele[3], Ralf Reski[1,4,*]

[1] Plant Biotechnology, Faculty of Biology, University of Freiburg, Schaenzlestrasse 1, 79104 Freiburg, Germany

[2] Cell Biology, Faculty of Biology, University of Freiburg, Schaenzlestrasse 1, 79104 Freiburg, Germany

[3] Molecular Botany, Department of Biology, Technical University of Kaiserslautern, Erwin-Schrödinger-Strasse 70, 67663 Kaiserslautern, Germany

[4] Signalling Research Centres BIOSS and CIBSS, Schaenzlestrasse 18, 79104 Freiburg, Germany

* Corresponding author: ralf.reski@biologie.uni-freiburg.de

Present address:

* Euro-BioImaging Bio-Hub, EMBL Heidelberg, Meyerhofstraße 1, 69117 Heidelberg, Germany

** Department of Anesthesiology, University Hospital Würzburg, Oberduerrbacher Strasse 6, 97072 Würzburg, Germany

*** Institute for Molecular Biosciences, Goethe University Frankfurt, Max-von-Laue-Str. 9, 60438 Frankfurt, Germany

**** Heraeus Medical GmbH, Philipp-Reis-Straße 8-13. 61273 Wehrheim, Germany

***** Eurofins GeneScan GmbH, Engesserstraße 4, 79108 Freiburg, Germany

****** Centre for Integrative Biodiversity Research (iDiv) Halle-Jena-Leipzig, Puschstrasse 4, 04103 Leipzig, Germany

ORCID-IDs S.N.W.H.: 0000-0002-2095-689X, B.Ö.: 0000-0001-9823-0581, N.v.G.: 0000-0002-0606-246X, A.A.M.: 0000-0003-1638-5438, B.R.v.B.: 0000-0002-9650-4064, L.N.: 0000-0003-0716-7236, J.S.F.: 0000-0002-5602-3901, R.K.: 0000-0002-3142-0863, S.G.: 0000-0002-2305-4525, T.W.: 0000-0002-9584-5449, F.S.: 0000-0001-5825-6621, M.R.F.: 0000-0003-1183-2075, S.J.M.S.: 0000-0003-4061-1175, R.R.: 0000-0002-5496-6711

Key words aging, Arabidopsis, Physcomitrella, Physcomitrium, protein oxidation, ROS

Abstract

Reactive oxygen species (ROS) are constant by-products of aerobic life. In excess, ROS lead to cytotoxic protein aggregates, which are a hallmark of ageing in animals and linked to age-related pathologies in humans. Acylamino acid-releasing enzymes (AARE) are bifunctional serine proteases, acting on oxidized proteins. AARE are found in all domains of life, albeit under different names, such as acylpeptide hydrolase (APEH/ACPH), acylaminoacyl peptidase (AAP), or oxidized protein hydrolase (OPH). In humans, AARE malfunction is associated with age-related pathologies, while their function in plants is less clear. Here, we provide a detailed analysis of AARE genes in the plant lineage and an in-depth analysis of AARE localization and function in the moss Physcomitrella and the angiosperm Arabidopsis. AARE loss-of-function mutants have not been described for any organism so far. We generated and analysed such mutants and describe a connection between AARE function, aggregation of oxidized proteins and plant ageing, including accelerated developmental progression and reduced life span. Our findings complement similar findings in animals and humans, and support a unified concept of ageing.

Introduction

Reactive oxygen species (ROS) are by-products of O_2 metabolism and a challenge to all aerobic life. ROS play a dual role as potentially lethal oxidants and as signalling molecules (Mittler et al., 2022). Therefore, aerobic organisms possess sophisticated redox systems to scavenge and detoxify excess ROS. The major sources of ROS in plant cells are the electron transport chains in mitochondria and plastids, but also in peroxisomes and at the plasma membrane (Tola et al., 2021). Environmental stresses such as heat, drought or high light intensities are factors for increasing ROS production to detrimental levels. Plants possess a repertoire of detoxifying enzymes such as catalases, superoxide dismutases, ascorbate peroxidases, glutathione peroxidase-like proteins and peroxiredoxins. Electrons for reduction are largely provided *via* non-enzymatic components such as ascorbic acid, glutathione and NADPH (Gratão et al., 2005; Smirnoff, 2000; Sharma et al., 2012; Müller-Schüssele et al., 2020; reviewed in Soares et al., 2019). In addition, a range of heat-shock proteins assist in disaggregation or refolding of damaged proteins (Parsell et al., 1994; Queitsch et al., 2000; reviewed in Mogk et al., 2018).

Despite conversion into non-toxic derivatives, the continuous exposure to ROS results in oxidation of DNA, lipids, and proteins (Sharma et al., 2012). On the protein level, ROS lead to irreversible cysteine oxidation, advanced glycation end-products, derivatives with ROS-generated lipid peroxides, and carbonylation of amino-acid side-chains (reviewed in Møller et al., 2007; Ciacka et al., 2020). If not cleared *via* proteolysis, an excess of oxidized proteins accumulates to cytotoxic protein aggregates. Plant antioxidant systems and the role of ROS as signalling molecules in abiotic stress responses are well studied (Farooq et al., 2019). Yet, factors involved in a plant cell's last line of defence, such as the proteolytic systems for the clearance of irreversibly oxidized proteins, are still underexplored.

A class of serine proteases is evolutionary deeply conserved as their activity is found in bacteria, archaea, animals and plants, and can degrade irreversibly oxidized proteins (Bartlam et al., 2004; Brunialti et al., 2011; Tsunasawa et al., 1975; Yamauchi et al., 2003). These proteases have different names in different organisms, e.g. acylamino acid-releasing enzyme (AARE), acylpeptide hydrolase (APEH/ACPH), acylaminoacyl peptidase (AAP), or oxidized protein hydrolase (OPH) (Rawlings et al., 2018) but are collectively addressed as AARE here. AARE acts in multimeric complexes (Yamauchi et al., 2003; Bartlam et al., 2004) as a bifunctional protease as it cleaves N^{α}-acetylated amino acids from oligopeptides *via* an exopeptidase mode, but also cleaves oxidized proteins *via* an endopeptidase mode (Tsunasawa et al., 1975; Fujino et al., 2000; Shimizu et al., 2003; Nakai et al., 2012; Gogliettino et al., 2014). AARE isoforms from various

organisms show different specificities towards N^{α}-acetylated amino-acids, with bacterial and archaeal enzymes preferring AcLeu and AcPhe substrates (Kiss et al., 2007; Szeltner et al., 2009; Brunialti et al., 2011; Gogliettino et al., 2012) and plant and animal isoforms preferring AcAla, AcMeth or AcGly substrates (Tsunasawa et al., 1975; Scaloni et al., 1992; Yamauchi et al., 2003; Riccio et al., 2015). Besides substrate specificities, their subcellular localization appears to be conserved among eukaryotes, as human (HsACPH) and Arabidopsis (AtAARE) AARE are reported as cytosolic enzymes (Shimizu et al., 2003; Nakai et al., 2012).

In humans, AARE malfunction is linked to different types of cancer (Scaloni et al., 1992; Gogliettino et al., 2021; Tangri et al., 2021) and sarcoma cell viability (Palumbo et al., 2016). Moreover, AARE and proteasomal activity correlate and cooperatively prevent cytotoxic aggregate formation (Shimizu et al., 2004; Palmieri et al., 2011; Bergamo et al., 2013). Several selective inhibitors have been identified (Yamin et al., 2009; Bachovchin et al., 2014) and blocking of AARE function is considered as anti-cancer treatment (Gogliettino et al., 2021). Despite an increasing number of studies on AARE functionality in humans, AAREs in plants are far less characterized.

AARE from *Arabidopsis thaliana* (AtAARE) and from cucumber have endo- and exopeptidase functions (Yamauchi et al., 2003), and silencing of AtAARE increased the levels of oxidized proteins (Nakai et al., 2012). AtAARE activity was also detected in plastid stroma fractions, although a fusion with a fluorescent reporter did not co-localize with chloroplasts (Nakai et al., 2012). Suppression of AtAARE *via* RNAi resulted in an enhanced accumulation of oxidized proteins in roots and enhanced electrolyte leakage in leaves, but a further impact on plant physiology was not described (Nakai et al., 2012).

Moreover, the complete loss of function of this protease has not yet been reported for any organism, neither bacterium, archaeon, animal, or plant. Thus, although the deep evolutionary conservation of AARE suggests its pivotal role in all major life forms, experimental evidence is far from optimal.

In a proteomics study on protein arginylation we identified an AARE homolog from the moss Physcomitrella (Hoernstein et al., 2016). Our further analysis revealed altogether three Physcomitrella AARE homologs (PpAARE1-3). Here, we analysed the subcellular localization of those PpAARE isoforms and of their homolog from the angiosperm Arabidopsis (AtAARE). We show that an alternative splicing event is targeting PpAARE1 to chloroplasts, mitochondria and the cytosol. We provide evidence that an alternative translation initiation is sufficient to localize

AtAARE to the same three subcellular compartments. Bioinformatic analyses of several genomes suggest that the localization of AARE in chloroplasts and mitochondria is conserved across the plant lineage. Employing combinatorial gene knockouts and protein co-immunoprecipitation we found distinct interactions between those three isoforms and their concerted action on progressive ageing in Physcomitrella. Likewise, an Arabidopsis AARE loss-of-function mutant exhibits enhanced levels of oxidized proteins and accelerated bolting, as a hallmark of plant ageing.

Results

AARE gene family expansion and splice variants

Previously, PpAARE1 (Pp1s619_3V6.1) was identified as the most prominent target for N-terminal arginylation in Physcomitrella (Schuessele et al., 2016; Hoernstein et al., 2016). N-terminal arginylation mediates poly-ubiquitination *via* the N-degron pathway, thus triggering subsequent proteasomal degradation (Varshavsky, 2019). Simultaneously, two homologs (PpAARE2: Pp1s108_134V6.1 and PpAARE3: Pp1s97_68V6.1) were identified, although those were not proven arginylation targets (Hoernstein et al., 2016). Meanwhile, a new Physcomitrella genome version with chromosome assembly and updated gene versions was released (Lang et al., 2018). Consequently, the gene accessions used here are PpAARE1 (Pp3c2_30720V3.1), PpAARE2 (Pp3c12_21080V3.1), and PpAARE3 (Pp3c7_25140V3.1). According to an *OrthoMCL* clustering (Chen et al., 2006) published in Zimmer et al. (2013), all three proteins are homologs of the *Arabidopsis thaliana* acylamino acid-releasing enzyme (AtAARE: AT4G14570, Yamauchi et al., 2003; Nakai et al., 2012). According to publicly available data (https://peatmoss.online.uni-marburg.de, Fernandez-Pozo et al., 2020) PpAARE1-3 are expressed in all major Physcomitrella tissues and developmental stages, although at varying levels (Fig. S1a). Except for leaves (phylloids) and spores, PpAARE1 is the most strongly expressed gene of this family (between 4 and 20 times). In contrast, PpAARE2 is expressed considerably stronger than PpAARE1 and PpAARE3 in spores (Fig. S1a). Likewise, AtAARE is expressed in all major Arabidopsis tissues (Fig. S1b, data utilized from Mergner et al. (2020) and downloaded from http://athena.proteomics.wzw.tum.de/). These data indicate a strong, positive correlation between transcript level and protein abundance across all tissues (Fig. S1b). Stress conditions result in a decreased AARE expression in Physcomitrella and Arabidopsis (Fig. S1c-e).

To investigate whether other plants also possess multiple AARE homologs and whether the PpAARE isoforms are inparalogs, we conducted *BLASTP* searches (Altschul et al., 1997) against

protein models from selected species using the protein sequence of AtAARE as a query. We selected the alga *Chlamydomonas reinhardtii* (Merchant et al., 2007), the liverwort *Marchantia polymorpha* (Bowman et al., 2017), the peat moss *Sphagnum fallax* (*Sphagnum fallax* v1.1, DOE-JGI, http://phytozome.jgi.doe.gov/), the lycophyte *Selaginella moellendorffii* (Banks et al., 2011), the monocot *Oryza sativa* (Ouyang et al., 2007) and the dicot *Populus trichocarpa* (Tuskan et al., 2006), all available at the Phytozome12 database (https://phytozome.jgi.doe.gov). Additionally, we performed a NCBI *BLASTP* search against the charophyte *Klebsormidium nitens* proteome (Hori et al., 2014), and identified a single homolog (GAQ80280.1) in this species. We also included proteins of *Funaria hygrometrica* (Kirbis et al., 2020), a close relative to Physcomitrella from the Funariacea family (Ostendorf et al., 2021), in our search. Finally, the AtAARE sequence was again searched against the Physcomitrella (Lang et al., 2018) and Arabidopsis proteomes (Lamesch et al., 2012). Homology of the resulting *BLAST* hits was confirmed if the reciprocal best *BLAST* hit against *A. thaliana* was again AtAARE.

In *P. trichocarpa*, we identified a single homolog for which three distinct splice variants are annotated (Potri.008G160400.1, Potri.008G160400.2, Potri.008G160400.3). These encode different protein isoforms, but two variants seem to encode non-catalytic proteins. AARE enzymes are prolyl-oligopeptidases with a conserved catalytic triad (Ser/Asp/His) in the C-terminal peptidase domain (Rawlings et al., 1991; Polgar, 2002). In splice variant 2 (Fig. S2, Potri.008G160400.2) alternative splicing results in the deletion of the catalytic Asp whereas the whole catalytic triad is lacking in splice variant 3 (Potri.008G160400.3). Hence, we consider these splice variants as non-active and disregard them from further discussion.

In rice, we identified two homologs (LOC_Os10g28020.3, LOC_Os10g28030.1), with an additional splice variant (LOC_Os10g28020.1) at one locus which encodes an N-terminal extension.

In *C. reinhardtii, M. polymorpha*, *S. fallax* and *S. moellendorffii*, we identified a single ortholog each. In *M. polymorpha*, three distinct splice variants are annotated (Mapoly0111s0036.1, Mapoly0111s0036.2, Mapoly0111s0036.3). The latter two are UTR splice variants, thus resulting in the same protein sequence, whereas Mapoly0111s0036.1 encodes an N-terminal extension of 97 aa compared to the other two variants. In *F. hygrometrica* we identified three distinct isoforms.

Finally, our *BLASTP* searches using the latest Physcomitrella protein models (Lang et al., 2018) confirmed three homologs of AtAARE (Pp3c2_30720V3.1, Pp3c12_21080V3.1, Pp3c7_25140V3.1). Additionally, this search revealed another hit, Pp3c1_2590V3.1. This gene

is composed of a single exon and encodes a 131 aa protein which harbours the AARE N-terminal domain (PF19283). However, it lacks a catalytic peptidase domain and is hardly expressed across different culture conditions and tissues (Perroud et al., 2018). We also did not find any proteomics evidence across several Physcomitrella analyses (Mueller et al., 2014; Fesenko et al., 2015; Fesenko et al., 2016; Hoernstein et al., 2016) for this protein. Therefore, we excluded this gene from further analysis.

We then used phylogenetic reconstruction to investigate the origin of gene duplications within the gene family. As an outgroup, we included the well-characterized rat and human AARE (Tsunasawa et al., 1975; Scaloni et al., 1992) and two isoforms of the Antarctic icefish *Chionodraco hamatus* (Riccio et al., 2015). Physcomitrella and *F. hygrometrica* share three distinct pairs of orthologs hinting at an expansion in the common ancestor of the two species. Our phylogenetic analysis did not resolve AARE subfamilies across kingdoms (Fig. 1a) and we conclude that the gene family expansions observed in rice and in the Funariaceae are lineage-specific events.

In addition, this analysis reveals a closer relationship between PpAARE1 and PpAARE3, which presumably originate from a more recent gene duplication event, compared to PpAARE2. This is supported by the fact that the open reading frames (ORFs) of PpAARE1 and PpAARE3 are represented by a single exon whereas the ORF of PpAARE2 is split across 17 exons, similar to AtAARE (Fig. 1b).

Eleven splice variants are annotated for PpAARE2, but they differ only in the splicing of the UTRs, whereas the translated proteins remain unaffected. The same situation is present for PpAARE3 where nine splice variants are annotated, which only differ in their UTR definitions. In contrast, three splice variants are annotated for PpAARE1 giving rise to two distinct protein isoforms (Fig. 1b; PpAARE1_1, PpAARE1_2). Both splice variants are present in Physcomitrella protonema (Fig. 1b, c), according to RT-PCR with splice variant-specific primers (Table S1).

Likewise, for AtAARE two different ORF definitions do exist. With Araport11 (Cheng al., 2017), a new version of the gene model was introduced exhibiting a longer ORF at the 5’ end and decreasing the size of the previously annotated 5’ UTR (Fig. 1b). We detected the full-length transcript *via* RT-PCR (Fig. 1c).

For PpAARE1, alternative splicing in the 5’ end results in an N-terminal truncated variant whereas the longer non-spliced variant encodes an N-terminal plastid transit peptide according to *TargetP2.0* (Armenteros et al., 2019; Fig. 1d). A cleavage of the transit peptide at the predicted

cleavage site (Ala^{72}-M^{73}, Table S2) of PpAARE1 would release exactly the protein encoded by the short splice variant. In contrast, PpAARE2 and PpAARE3 do not harbour any predicted N-terminal targeting signal. Moreover, PpAARE3 is also lacking the WD40 domain that is present in PpAARE1 and PpAARE2 (Fig. 1d).

The extension of the originally annotated ORF of AtAARE also encodes a plastid transit peptide (Fig. 1d) according to *TargetP2.0*. To our knowledge, the longer variant of AtAARE has not yet been investigated, whereas the short variant of AtAARE localizes to the nucleus and the cytosol (Nakai et al., 2012). In agreement with the latter findings, we could predict an NLS (KKKK) with *LOCALIZER* (Sperschneider et al., 2017). Thus, targeting of AtAARE to the cytosol and the nucleus, but also to plastids could be enabled by alternative translation initiation.

Accordingly, we checked for NLS in PpAARE isoforms and found one (KRRP, Table S2) in PpAARE1 and PpAARE3, whereas PpAARE2 has none, further supporting our hypothesis that PpAARE1 and PpAARE3 originate from a relatively recent gene duplication event.

Alternative splicing also generates two distinct transcripts for AARE1 in rice (OsAARE1, Table S2), where one variant encodes a potential plastid transit peptide resembling PpAARE1. Poplar AARE (PtAARE) also harbours a plastid transit peptide. Here, an alternative translation start site as observed for AtAARE could be possible as a methionine is also present around the predicted targeting peptide cleavage site. However, we did not find any evidence for alternative translation initiation. For all other plant species, no plastid targeting sequence was predicted, while the *C. reinhardtii* AARE harbours a mitochondrial targeting sequence (Table S2).

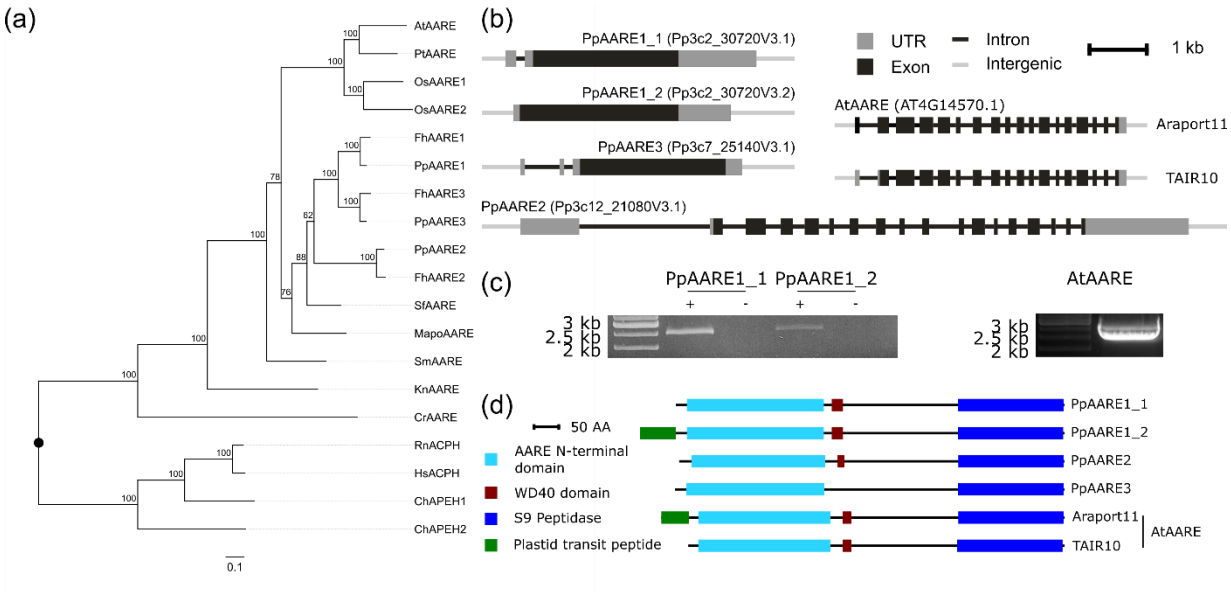

Fig. 1 Phylogenetic tree for AARE isoforms from selected organisms, gene structures and proteins domains of *P. patens* and *A. thaliana* AARE isoforms. (a) Maximum likelihood tree based on an alignment of multiple AARE coding sequences. Duplication events in several species appear to be lineage-specific. Node values reflect percentage confidence values based on 1000 bootstrap replicates. Species abbreviations: At: *Arabidopsis thaliana*; Pt: *Populus trichocarpa*; Os: *Oryza sativa*; Pp: *Physcomitrium patens*; Fh: *Funaria hygrometrica*; Sf: *Sphagnum fallax*; Mp: *Marchantia polymorpha*; Sm: *Selaginella moellendorffii*; Kn: *Klebsormidium nitens*; Cr: *Chlamydomonas reinhardtii*; Rn: *Rattus norvegicus*; Hs: *Homo sapiens*; Ch: *Chionodraco hamatus*. (b) Gene structure of PpAARE1-3 and AtAARE. For PpAARE1 two splice variants exist. For AtAARE two different 5' UTR definitions are present (upper: Araport11 (Cheng et al., 2017); lower: TAIR10 (Lamesch et al., 2012)). (c) Left: Both splice variants of PpAARE1 were amplified from cDNA (+: with cDNA template; -: without reverse transcriptase). Expected amplicon size: PpAARE1_1: 2512 bp; PpAA1_2: 2596 bp. Primers were designed to be specific for the splice variants (Table S1). Right: The longer open reading frame of AtAARE was amplified from cDNA. Expected amplicon size: 2457 bp (Table S1). (d) Protein structures showing PFAM-domains for PpAARE1-3 and AtAARE. All isoforms contain AARE N-terminal domain (PF19283) and a catalytic Peptidase S9 domain (PF00326). PpAARE1, PpAARE2 and AtAARE additionally contain a WD40 domain (PF07676). The long splice variant of PpAARE1 and the longer open reading frame of AtAARE encode a predicted N-terminal plastid transit peptide (cTP). AA: amino acid. Cleavable N-terminal sequences were predicted by *TargetP2.0* (Armenteros et al., 2019).

PpAARE1 and AtAARE in mitochondria, chloroplasts and cytoplasm

Organellar targeting of AARE has not yet been reported, although Yamauchi et al. (2003) observed AARE activity in plastid-enriched fractions of cucumber. However, chloroplasts, peroxisomes and mitochondria are major hubs of ROS generation (Waszczak et al., 2018), and thus are likely organelles with elevated levels of oxidized proteins. Thus, we investigated whether PpAARE1 and AtAARE would localize to chloroplasts *in vivo*.

Therefore, we generated fusion constructs of the PpAARE isoforms and of AtAARE with eGFP for transient expression in Physcomitrella protoplasts. Due to the presence of a predicted plastid targeting peptide for PpAARE1, eGFP was fused in frame to the 3' end of all CDSs. Since also peroxisomes are ROS-producing organelles, we used *PlantPredPTS1* (Lingner et al., 2011; Reumann et al., 2012) to check for the presence of C-terminal positioned peroxisomal targeting signals. None of the selected AARE isoforms was predicted to localize to peroxisomes (Table S2). Although AtAARE has a C-terminal CKL tripeptide, which is experimentally verified to mediate peroxisomal targeting (Gould et al., 1989; Lingner et al., 2011), the properties of its other C-terminal amino acids most likely prevent peroxisomal targeting. A more recent prediction approach for PTS1-mediated targeting for Arabidopsis proteins (Wang et al., 2017) further supports this conclusion. Peroxisomal targeting can also be mediated *via* N-terminal nona-peptides (Petriv et al., 2004; Reumann, 2004), but these motifs are also not present within the first 100 aa in any of the selected AARE sequences. In agreement with these predictions eGFP was fused to the 3' end of the CDSs.

For PpAARE1 three different fusion constructs were assembled. Among these, a fusion of the CDS of the short splice variant (Pp3c2_30720V3.1) and eGFP was cloned as well as a fusion of the CDS of the longer splice variant (Pp3c2_30720V3.2) and eGFP. Additionally, we cloned a fusion of eGFP and the sequence part in which both variants differ (M^1-A^{72}, Pp3c2_30720V3.2). This differing sequence part harbours the plastid transit peptide predicted by *TargetP2.0*. All fusion constructs were expressed under the control of the Physcomitrella Actin5 promoter (Weise et al., 2006; Mueller et al., 2014) in a pMAV4 plasmid backbone as described in Özdemir et al. (2018).

The PpAARE1 isoform derived from the short splicing variant (PpAARE1_1, Fig. 1b) clearly localized to the cytoplasm (Fig. 2). The same localization was observed for PpAARE2 and PpAARE3 (Fig. 2). Despite a predicted NLS, we did not observe a nuclear localization, either for PpAARE1 or for PpAARE3.

The isoform encoded by the longer splice variant of PpAARE1 (PpAARE1_2, Fig. 1b) localized to chloroplasts and surprisingly also to mitochondria (Fig. 2). In contrast to the diffuse cytosolic distribution of PpAARE1, specific foci were observed in chloroplasts. To investigate whether the N-terminal sequence differing between the two PpAARE1 variants (M^1-A^{72}, Pp3c2_30720V3.2) is sufficient to confer dual targeting, we fused this N-terminal sequence 5' to eGFP and observed again dual localization (Fig. 2, PpAARE1_Nt). Full-length PpAARE1 was necessary to localize eGFP to foci within chloroplasts, as the PpAARE1_Nt:eGFP fusion led to a uniform distribution. However, full-length PpAARE1 was also homogeneously distributed throughout the cytoplasm. This indicates the presence of interactors that recruit PpAARE1 to specific sites or complexes within the chloroplasts. Further, we conclude that the N-terminal extension of PpAARE1_2 encodes an ambiguous targeting signal for import into chloroplasts and mitochondria as it is capable of localizing the fusion protein simultaneously to both organelles.

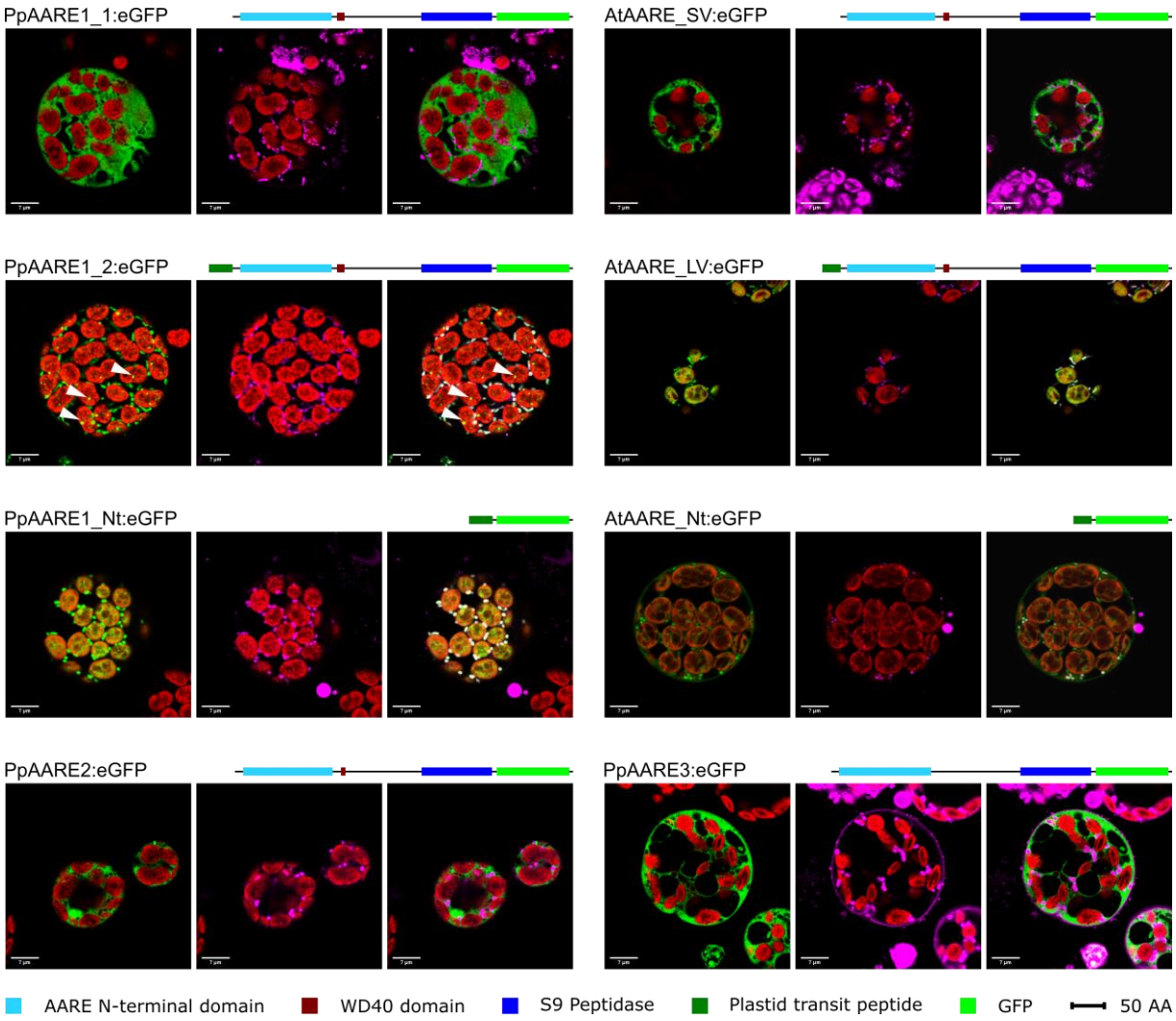

Fig. 2 Confocal microscopy images showing the localization of PpAARE isoforms and AtAARE with C-terminally fused eGFP in Physcomitrella protoplasts. Fusion proteins with domain structures are depicted. Green: eGFP. Red: chlorophyll. PpAARE1_1, PpAARE2 and PpAARE3 localize to the cytoplasm. PpAARE1_2 localizes to specific foci in plastids (white arrows) and to mitochondria. The N-terminal extension of PpAARE1_2 encoding a predicted plastid transit peptide (PpAARE1_Nt) directs eGFP to plastids and mitochondria. The short variant of AtAARE (SV) localizes to the cytoplasm. The long variant (LV) localizes to plastids and mitochondria. The N-terminal extension of the long variant of AtAARE localizes to plastids and mitochondria. Left image: eGFP (green). Middle image: chlorophyll autofluorescence (red) and MitoTracker™ (magenta). Right image: chlorophyll autofluorescence (red), eGFP (green), Mitotracker™ (magenta) and co-localization of eGFP and MitoTracker™ (white). Bars = 7 µm.

Based on this data, PpAARE1 is targeted to three different organelles: chloroplasts, mitochondria and the cytosol. To independently scrutinize these findings, we measured AARE enzyme activity in the organelles. Using organelle fractionation as previously described (Lang et al., 2011), we detected AARE activity in chloroplasts, the cytosol, and mitochondria, although to a lesser extent in the latter (Fig. S3). Thus, *in vivo* localization of fusion proteins and enzyme measurements after cell fractionation independently confirm the predicted triple localization of AARE in Physcomitrella.

Simultaneous localization of proteins to chloroplasts and mitochondria can be mediated *via* ambiguous targeting signals which are recognized by both translocation machineries. We evaluated whether *ATP2* (Fuss et al., 2013), a tool for the prediction of ambiguous targeting, would recognize PpAARE1 but this was not predicted to be dually targeted. In contrast, AtAARE was predicted to be dually targeted *via* an ambiguous signal. Thus, we cloned the analogous three fusion constructs for AtAARE and investigated the subcellular localization of their encoded proteins accordingly.

The AtAARE isoform translated from the shorter ORF (AtAARE, Fig. 1b) localized to the cytoplasm (AtAARE_SV, Fig. 2), as observed for PpAARE1_1. This result is partially in agreement with Nakai et al. (2012) since we could not observe nuclear localization. Using the fusion construct of the longer AtAARE variant, we observed clear dual targeting of the protein to chloroplasts and mitochondria (AtAARE_LV, Fig. 2), as observed for PpAARE1_2. Here, the eGFP signal was distributed homogeneously in the chloroplasts, in contrast to the foci of PpAARE1:eGFP.

Next, we cloned only the N-terminal sequence differing between both variants (M^1-A^{55}, longer ORF definition, Fig. 1b) and fused it to eGFP. In order to investigate whether the exact N-terminal difference between the two AtAARE variants would be sufficient for targeting, the M^{56} (same as M^1 in the shorter variant), which is the P1 aa at the predicted cleavage site, was deleted. Using this construct, the eGFP signal localized to chloroplasts and mitochondria (AtAARE_Nt, Fig. 2). The signal within chloroplasts was homogeneously distributed, similar to the longer AtAARE variant. Thus, we conclude that the N-terminal extension of both long PpAARE and AtAARE variants is sufficient for dual targeting of proteins *in vivo*. Intriguingly, the longer variant of AtAARE localized exclusively to chloroplasts and mitochondria although alternative translation initiation should be possible. This is interesting as alternative translation initiation is also possible in the longer splice variant of PpAARE1 (PpAARE1_2). But in the latter also the fusion protein localizes exclusively to chloroplasts and mitochondria, which excludes the possibility of an alternative translation initiation, at least in protoplasts. There are numerous transcripts in mammals where translation of an upstream positioned ORF suppresses the translation of the downstream main

ORF (Orr et al., 2020). A similar scenario is conceivable in Physcomitrella. However, it remains unclear how and if translation from the internal start codons is controlled. It is also possible that factors controlling alternative translation initiation of AtAARE are absent in Physcomitrella, at least in a spatiotemporal manner, or they might only be triggered at specific physiological situations. According to our data, the translation of the two variants of PpAARE1 is mainly controlled by alternative splicing and not by alternative translation initiation.

In summary, PpAARE1 and AtAARE localize to three subcellular compartments *via* an ambiguous targeting signal. In contrast, PpAARE2 and PpAARE3 localize solely to the cytoplasm.

Double knockout of PpAARE1/2 reduces lifespan

Null mutants of AARE have not been described in any organism, and the biological role of this protease apart from its catalytic function remained unclear. Hence, we created AARE knockouts in Physcomitrella by deleting the full CDS of each gene *via* gene targeting (Fig. 3a) according to Hohe et al. (2004). To enable subsequent knockout (KO) of other AARE genes, different selection markers were used. Since three distinct AARE genes do exist in Physcomitrella which result in cytosolic proteases, we generated all possible combinations of double KOs and triple KOs to avoid potential compensation of the loss of function.

Plants surviving the selection procedure were screened *via* PCR for the absence of the respective CDS and correct integration of the KO construct in the target locus (Fig. S4a). Additionally, the number of genomic integrations of the KO construct was measured *via* qPCR as described in Noy-Malka et al. (2014) (Fig. S4b). At least three independent lines were identified for all single, double and triple KOs (Fig. S4c-i) and a line with only a single integration in the genome was detected for each KO (j-p, line numbers with stars). Further, haploidy of all lines was confirmed *via* flow cytometry (Fig. S5a-c) according to Heck et al. (2021). We used lines with a single integration of the KO construct (Fig. S4) for subsequent experiments.

Typically, AARE exopeptidase activity is proven *via* N^{α}-acetylated amino acids like AcAla or AcMet coupled to a reporter such as para-nitro-anilide (pNA) or 7-amido-4-methylcoumarin (AMC). From these, AcAla-pNA was tested for several eukaryotic AAREs, including AtAARE (Scaloni et al., 1992; Yamauchi et al., 2003; Gogliettino et al., 2014). Here, we analysed the impact of AARE loss of function on the activity towards AcAla-pNA and AcLeu-pNA. The latter is a substrate of bacterial and archaeal AARE isoforms but also eukaryotic isoforms exhibit cleavage activity on this

substrate (Tsunasawa et al., 1975; Kiss et al., 2007; Szeltner et al., 2009; Brunialti et al., 2011; Gogliettino et al., 2012; Gogliettino et al., 2014). On the single KO level, the exopeptidase activity on both substrates is significantly reduced in the ∆PpAARE1 mutant whereas the single KO of the other isoforms did not affect the activity (Fig. 3b). This strong impact of PpAARE1 on the exopeptidase activity is consistent across all transgenic mutant lines (Fig. S6).

One important step in Physcomitrella development is the transition from protonema to gametophores, a developmental progression regulated among others by plant age and the nutrient status (Lorenz et al., 2003). The single KOs are phenotypically inconspicuous on the gametophore level (Fig. 3c). In contrast, gametophores of ∆PpAARE1/2 and ∆PpAARE1/3/2 are severely stunted and colonies are denser compared to WT or the other mutants (Fig. 3c). This growth effect is restricted to gametophores since protonema growth on solid medium does not differ between WT and the KOs (Fig. 3d, e). Intriguingly, ∆PpAARE1/2 and ∆PpAARE1/3/2 mutants showed accelerated developmental transition, as they developed gametophores from protonema earlier (Fig. 3d). Since other KO lines do not show this effect, we attribute this to the double KO of PpAARE1/2 and performed a quantitative comparison with WT. Here, gametophores were already observed after 6 days in the double KO of PpAARE1/2, while in WT a similar number of gametophores per colony was observed only after 13 days (Fig. 3f). Consequently, the double KO of PpAARE1/2 causes accelerated developmental progression but gametophores remain ultimately smaller than in WT (Fig. 3c). These effects are not linked to AARE exopeptidase activity since the exopeptidase activity in gametophores is significantly reduced in all lines with a KO of PpAARE1 (Fig. 3g), which mimics the activity profile in protonema (Fig. S6).

To analyse AARE endopeptidase activity, we assessed the total levels of oxidized proteins in gametophores. In this assay, protein carbonyl groups derived from oxidation are derivatized with 2,4-dinitrophenylhydrazine (DNPH) to 2,4-dinitrophenylhydrazone (DNP). This irreversible modification is then recognized on Western blots by a primary anti-DNP antibody. Since DNPH can also react with oxidation states of cysteine side chains (Dalle-Donne et al., 2009), this assays not only protein carbonylation but general protein oxidation.

With this assay we found that PpAARE2 had the strongest impact on the level of oxidized proteins in gametophores (Fig. 3h) and thus is not linked to exopeptidase activity. This was consistently observed in three independent analyses (Fig. 3h, Fig. S7). Apparently, PpAARE3 does not have any impact on exopeptidase and endopeptidase activity in gametophores under standard conditions (Fig. 3g, h).

Taken together, PpAARE1 predominantly acts as exopeptidase, while PpAARE2 predominantly acts as endopeptidase, and only the simultaneous loss of both activities in the double knockout mutants has the severest phenotypical consequences.

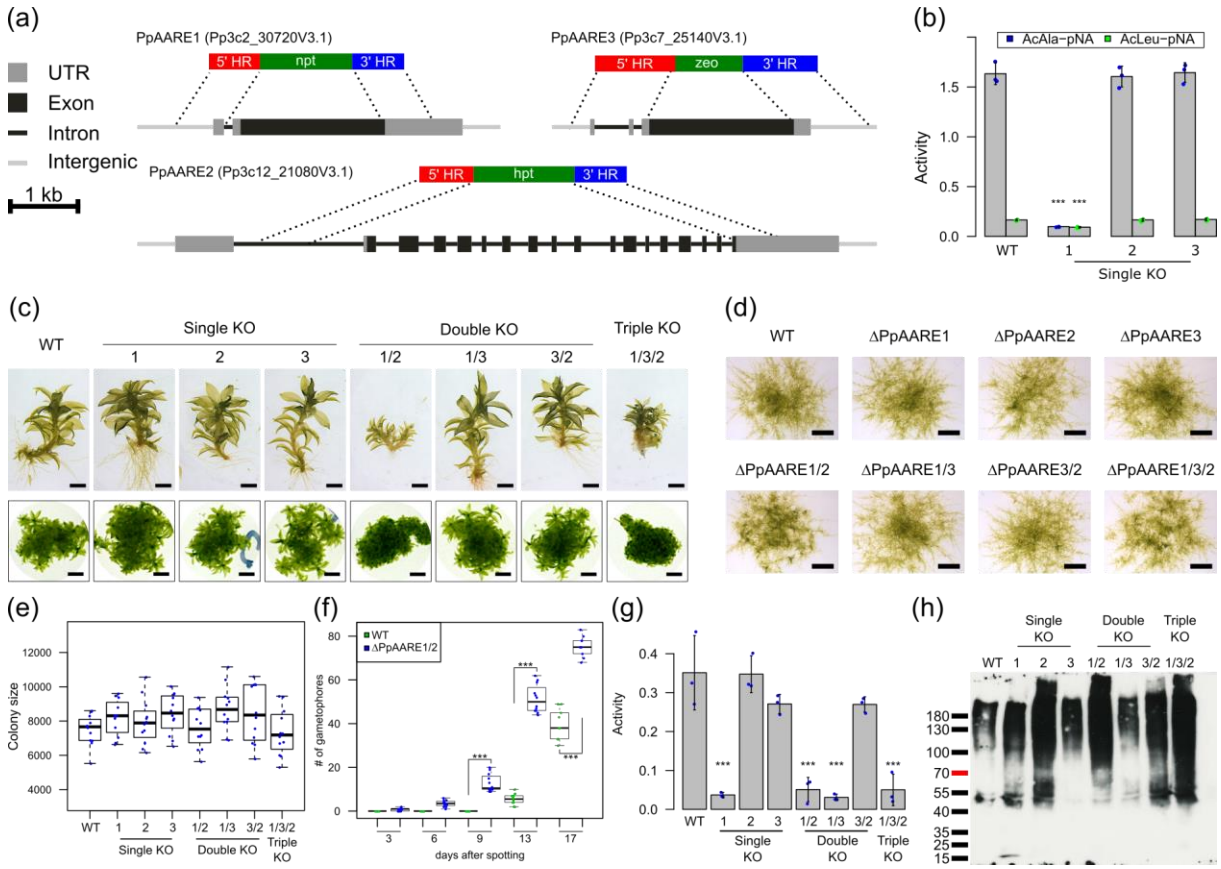

Fig. 3 Phenotypes, AARE activity and level of oxidized proteins in Physcomitrella WT and all types of KO mutants. (a) Each isoform was knocked out using a different selection marker. The selection markers confer resistance against G418 (npt), hygromycin (hpt) and zeocin (zeo), respectively. Homologous regions (HR) were chosen in order to remove the full CDS of the corresponding gene upon integration of the selection marker. (b) Mean AARE activity on AcAla-pNA in Physcomitrella protonema with standard deviation (n= three biological replicates). Significance levels are based on a one-way Anova and subsequent post-hoc test (***: $p<0.001$) and indicate differences compared to WT. (c) Phenotypes of gametophores of WT and the different KOs cultivated on KnopME for 4 months. All colonies were grown on the same plate. Upper panel: Bar = 0.5 mm; lower panel: Bar = 2mm. (d) Protonema colonies grown on KnopME with 0.02% glucose spotted from suspension culture (440 mg DW/L). Bar = 1 mm. Images were

taken 9 days after spotting. (e) Box plot showing the distribution of colony areas (n = 12 colonies per boxplot; colony images taken 7 days after spotting). No significant difference of colony areas between WT and the KOs was observed (tested via one-way Anova). (f) Box plot showing the number of gametophores per colony and day of WT and ΔPpAARE1/2. Counting was performed at indicated days after spotting protonema suspension culture on solid medium (KnopME with 0.02% glucose). Indicated significance levels are based on a two-way Anova with subsequent post-hoc test (***: $p<0.001$). (g) Mean AARE exopeptidase activity on AcAla-pNA in gametophores. Depicted is the mean of three independent colonies per line with standard deviations. All colonies were cultivated on the same plate (Fig. S7a). Significance levels are based on one-way Anova and indicate differences compared to WT (***: $p<0.001$). (h) Levels of oxidized proteins in gametophores of WT and the different KOs (Coomassie-stained loading control is available (Fig. S7b). The analysis was repeated in three times (additional Blots available in Fig. S7c, d). Detection of oxidized proteins was performed with the OxyBlot™ *Protein Oxidation Detection Kit* (Merck).

We found another remarkable difference between WT and mutants with a double KO of PpAARE1/2 in older plants. After 5 months of cultivation, ΔPpAARE1/2 and ΔPpAARE1/3/2 were only viable at the tip of the gametophores (Fig. 4a), whilst most of the colony was already dead. In contrast, gametophores of WT and the other KOs were fully viable. After 8 months, ΔPpAARE1/2 and ΔPpAARE1/3/2 were already dead, in contrast to WT and the respective parental lines, which only showed some dead gametophores (Fig. 4b, c).

In summary, mutants with a double KO of PpAARE1/2 exhibit accelerated developmental transition from protonema to gametophore (Fig. 3f), while size and life span of gametophores is strikingly reduced (Fig. 3c, Fig. 4a-c). In contrast, these effects are not visible in ΔPpAARE1/3. Therefore, these ageing phenotypes are linked to the concurrent loss of major AARE endopeptidase and exopeptidase activity.

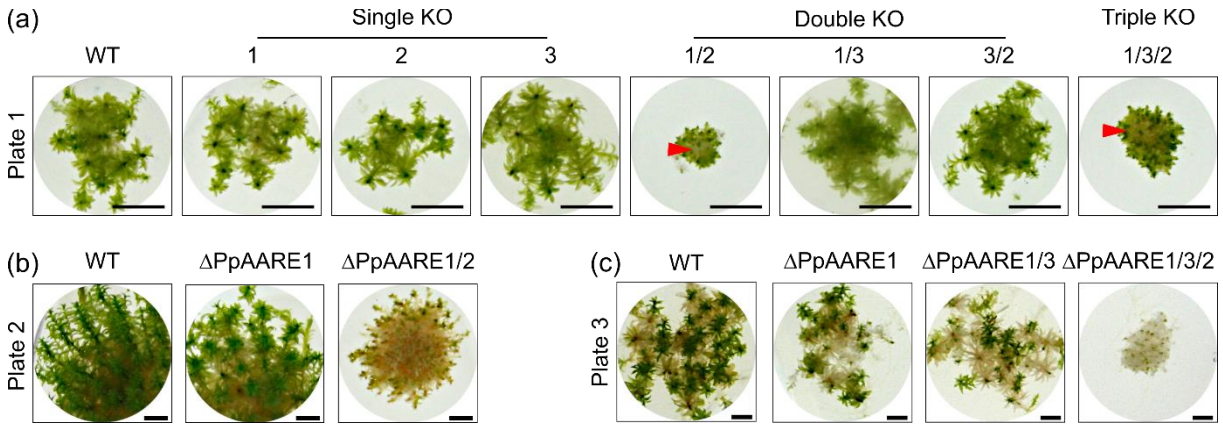

Fig. 4 Physcomitrella gametophore colonies of varying age. (a) Colonies of all representative knockout mutants after 5 months on solid medium (KnopME). Bar = 5 mm. Gametophores of ΔPpAARE1/2 and ΔPpAARE1/3/2 are only viable at the tip, whereas plant material at the base (red arrow) is dead. (b) Colonies after 8 months on solid medium. ΔPpAARE1 is the parental line for ΔPpAARE1/2. Gametophores of WT and ΔPpAARE1 are still viable whereas ΔPpAARE1/2 gametophores are mostly dead. Bar = 2 mm. (c) Colonies after 8 months on solid medium. ΔPpAARE1 is the parental line for ΔPpAARE1/3 and ΔPpAARE1/3 is the parental line for ΔPpAARE1/3/2. Colonies of WT, ΔPpAARE1 and ΔPpAARE1/3 still have viable gametophores, whereas ΔPpAARE1/3/2 gametophores are dead. Bar = 2 mm.

Distinct *in vivo* interactions of PpAARE isoforms

In different organisms, AARE forms different homomeric complexes such as dimers (Bartlam et al., 2004), tetramers (Yamauchi et al., 2003), or hexamers (Szeltner et al., 2009). Thus, we analysed whether the PpAARE isoforms can interact with each other. In a previous study, all three isoforms were identified, although the protein modification used for pulldown (N-terminal arginylation) was only identified on PpAARE1 (Hoernstein et al., 2016). This stimulated two hypotheses: First, PpAARE2 and PpAARE3 are also targets for N-terminal arginylation, but modified peptides were not identified for these isoforms. Second, the isoforms interact in complexes which were pulled down due to the N-terminal arginylation of PpAARE1. We generated Citrine fusion lines for each isoform *via* in-frame tagging at the native locus (knock-in, Fig. 5a). The original stop codons of the respective PpAARE CDS were deleted. The Citrine-tag was intended for two different analyses: First, it should enable *in vivo* monitoring of PpAARE isoforms expressed from the native promoter, and second, it is a valid tag for co-immunoprecipitation (Co-IP) *via* commercially available trap-beads.

In plants with a detectable fusion transcript (Fig. S8a-c) the presence of the target protein was checked *via* IP and subsequent MS analysis. For PpAARE3:Citrine lines, we detected transcripts in one line and obtained only insufficient coverage and intensity at the MS across several Co-IPs. Thus, these Physcomitrella lines were excluded from further analysis. The co-precipitation of other PpAARE isoforms with the respective bait isoforms was observed in test IPs (Fig. S8d-e) confirming the MS-Data of Hoernstein et al. (2016). All plants harbouring the Citrine fusion were phenotypically inconspicuous (Fig. S8f) and haploid (Fig. S8g). Although the fusion proteins were detected in two independent lines for each of the two isoforms (PpAARE1, PpAARE2), we could not observe any Citrine signal within Physcomitrella protonemata or gametophores, probably due to the low abundance of the PpAARE isoforms. Nevertheless, MS intensities and sequence coverage enabled quantitative Co-IPs.

When targeting PpAARE1:Citrine, both other isoforms appeared as significant interacting partners (Fig. 5b, $p < 0.01$, FDR = 0.01). In a reciprocal Co-IP targeting PpAARE2:Citrine only, PpAARE1 appeared as significant interacting partner. PpAARE3 was not detected in this pulldown. Although lacking a reciprocal IP targeting PpAARE3:Citrine, the data show that PpAARE1 interacts with PpAARE2 and PpAARE3, whereas PpAARE2 only interacts with PpAARE1. Consequently, there are distinct interactions of PpAARE1 with PpAARE2 and PpAARE3 *in vivo*, possibly resulting in cytosolic heteromeric AARE complexes in Physcomitrella.

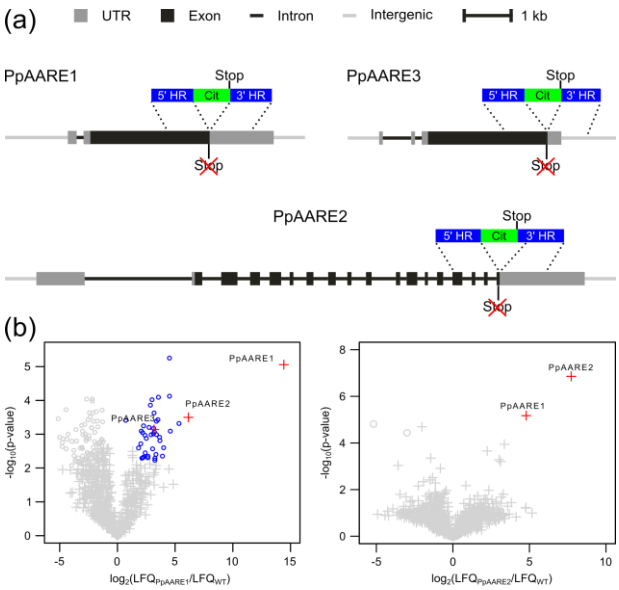

Fig. 5 Reciprocal co-immunoprecipitation (Co-IP) with Citrine-tagged PpAARE isoforms. (a) Tagging of PpAARE isoforms was realized by in-frame fusion with a linker-Citrine CDS at the

respective native locus *via* homologous recombination. Original stop codons were deleted. (b) Volcano plots showing the result of the Co-IPs against each of the PpAARE:Citrine fusion proteins. Left panel: Pulldown of PpAARE1:Citrine. Right panel: Pulldown of PpAARE2:Citrine. Co-IP was performed with GFP-Trap Magnetic Particles M-270 (Chromotek) and protonema from suspension culture. Log_2 ratios of normalized label-free quantitation values (LFQ) are plotted against $-log_{10}$ of adjusted p-values. Proteins significantly enriched in the Citrine tagged pulldown are shown in blue circles ($p < 0.01$, FDR = 0.01). Significantly enriched PpAARE isoforms are depicted as red crosses.

Accelerated bolting in Arabidopsis

In Physcomitrella, three AARE genes exist, and the concerted action and interaction of the enzymes affect plant ageing. To evaluate if this is an evolutionary conserved function, we analysed the situation in Arabidopsis. Here, it was known that silencing of the single AARE gene leads to an accumulation of oxidized proteins, whereas overexpression did not affect their levels (Nakai et al., 2012). To gain deeper insights, we screened for available Arabidopsis T-DNA mutants.

We identified two T-DNA insertion lines (SALK_071125 and GK-456A10) in the T-DNA Express database at the SIGnAL website (http://signal.salk.edu). SALK_071125 (s68) has a T-DNA insertion in an intron of the 5´UTR, whereas the T-DNA insertion in GK-456A10 (GK) maps to an intron in the region encoding the catalytic domain (Fig. 6a). We obtained these mutants, identified homozygous populations of GK-456A410 containing the T-DNA insertion by their resistance to sulfadiazine, and confirmed their genotype by PCR. In the case of the Salk line (s68), homozygous plants had lost their resistance to kanamycin, but we could confirm their genotype by PCR.

Homozygous plants of both genotypes were back-crossed with WT Col-0, and brought to homozygosis for subsequent experiments. Primers for screening and validation of both T-DNA lines are listed in Table S3. Additionally, we analysed AARE gene expression *via* RT-PCR. The transcript was still detectable in both lines (Fig. 6a), although very reduced in s68, while the protein was not detectable *via* Western blot (Fig. 6b). Surprisingly, in WT AARE was detected at around 100 kDa, although the estimated molecular weight is approximately 84 kDa (90 kDa for the longer ORF variant without cleavage of the plastid targeting peptide) which indicates the presence of posttranslational modifications. Phenotypically, neither seedlings nor adult mutant plants showed obvious deviations from WT (Col, Fig. S9)

Next, we assayed AARE exopeptidase function in Arabidopsis WT and the two mutants. The exopeptidase activity on AcAla-pNA was significantly reduced in both T-DNA mutants. In contrast, the activity on AcLeu-pNA did not change significantly, although a slight reduction was observed in the GK line (Fig. 6c). Thus, in agreement with Western blot and activity data, the remaining transcripts detected *via* RT-PCR (Fig. 6a) are not translated to functional enzymes, suggesting complete loss of AARE function in the mutants. Based on this characterization, we concentrated on T-DNA mutant s68.

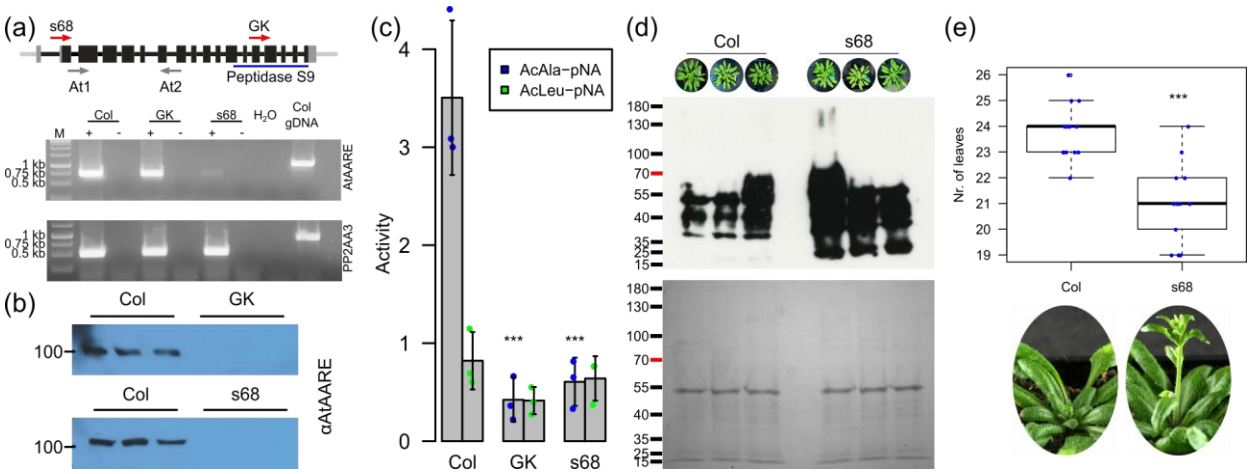

Fig. 6 Molecular and phenotypical characterization of *A. thaliana* T-DNA mutant lines. (a) Structure of the AtAARE gene and positions of T-DNA insertions (red arrows indicate positions of T-DNA insertion, s68 (SALK_071125) and GK (GK-456A10)) and primers (At1, At2) used for RT-PCR (below). Transcription analysis of AtAARE was performed by RT-PCR in WT (Col), s68, and GK plants. Negative controls without reverse transcriptase (-), a water control (H_2O) and genomic DNA control (gDNA) are indicated. Expected amplicon sizes: AtAARE: cDNA 739 bp, gDNA: 1204 bp; PP2AA3 (reference gene): cDNA: 517 bp, gDNA: 911 bp. Primers are listed in Table S3. (b) Western blot analysis on extracts of the two T-DNA mutants and WT probed with a polyclonal @AARE antibody. In both T-DNA lines AtAARE is not detectable. (c) Mean exopeptidase activity in *A. thaliana* extracts on AcAla-pNA and AcLeu-pNA with standard deviation (n = 3 biological replicates). Significance levels are based on one-way Anova and subsequent post-hoc test (***: $p<0.001$) and indicate differences compared to WT (Col). (d) Detection of oxidized proteins in WT (Col) and ΔAtAARE mutant (s68). From three independent plants one exterior rosette leaf was taken after cultivation for 8 weeks in short-day conditions (8h light/16h dark). Protein loading control by Coomassie staining is depicted below. (e) Boxplot of the bolting analysis of WT (Col, n

= 14) and AtAARE mutant plants (s68, n=13). Significance level is based on one-way Anova and subsequent post-hoc test (***: $p<0.001$). Exemplary plants (45-day-old plants grown in long-day conditions, 16h light/8h dark) are depicted below the boxplot.

Subsequently, we assayed the AARE endopeptidase activity in Arabidopsis. The most striking feature reported in Nakai et al. (2012) were increased levels of oxidized proteins in AARE-silenced Arabidopsis plants which is in line with our findings in Physcomitrella AARE mutants. To corroborate this, we investigated levels of oxidized proteins in the Arabidopsis T-DNA mutant (s68) in comparison to WT (Col). We analysed plants cultivated under short day conditions to delay bolting, which is the swift upward growth at the transition to flowering (Levey & Wingler, 2005). In both genotypes, the distribution of oxidized proteins was different to Physcomitrella gametophores (Fig. 6d). Using the same extraction protocol, oxidized proteins in Arabidopsis were mainly of lower molecular weight, whereas in Physcomitrella they were mainly at higher molecular weight (Fig. 3h). Despite these size differences, the level of oxidized proteins was higher in the Arabidopsis mutant than in WT (Fig. 6d), mimicking the situation in Physcomitrella. Together, we found AtAARE exopeptidase and endopeptidase activity in our experiments.

Johansson et al. (2004) analysed the levels of oxidized proteins during the Arabidopsis life cycle and observed an accumulation of oxidized proteins during vegetative growth, which was depleted at the transition to bolting. It was not clear from this study, whether the level of oxidized proteins is a signal for bolting, or if the reset of protein oxidation at the bolting transition is a side-effect of enhanced protein turnover during this process. To address this, we assessed the bolting behaviour of Arabidopsis WT and mutant plants and found that bolting in mutant plants differed significantly from WT. In WT, bolting started at 24±1 rosette leaves whereas it started already at 21±2 rosette leaves in the mutants (Fig. 6e). Consequently, this accelerated developmental transition in the mutants correlates with enhanced levels of oxidized proteins, which may act as a molecular signal for the transition from vegetative to generative phase as a major step in plant ageing.

Discussion

A universal definition of ageing is difficult due to strongly differing characteristics between and within the domains of life. In humans, the term ageing is inherently linked to degenerative diseases whereas plant ageing is considered as the progression of developmental transitions from seeds

to senescence. Nevertheless, a common feature of ageing is the execution of a genetic program that controls growth, development and maturation. In turn, the progression of this genetic program dependents on the metabolic state and environmental factors. Among the molecules responsible for ageing are ROS. Their involvement in ageing and diseases was first postulated by Harman (1956) and was extended by considering mitochondria as central sources (Harman, 1972). In humans, mitochondrial malfunction in line with increased ROS levels is a central determinant of ageing and associated pathologies (Giorgi et al., 2018). In plants, mitochondrial ROS increase during ageing of seeds (Mao et al., 2018) and are major determinants of germination capacity (Ratajczak et al., 2019). In photosynthetic tissues, chloroplasts are the major source of ROS, and their levels increase during ageing (Munné-Bosch & Alegre, 2002; Noctor et al., 2002; Foyer & Noctor, 2003). Plants cannot escape from stress situations that increase ROS production to detrimental levels, and despite several layers of ROS defence, oxidized proteins constitute the major share of modified molecules under stress. Consequently, protein oxidation and subsequent aggregate deposition are hallmarks of ageing (Sohal & Weindruch, 1996; López-Otín et al., 2013). The degradation of artificially oxidized proteins by AARE has been demonstrated repeatedly, and silencing of AtAARE in turn increased the levels of oxidized proteins (Fujino et al., 2000; Shimizu et al., 2003; Nakai et al., 2012; Goglíettino et al., 2014).

However, a contribution of AARE to the progress of ageing remained elusive, although several studies associate AARE-function to age-related diseases (Senthilkumar et al., 2001; Palmieri et al., 2017; Marshall et al., 2019). Here, we identify three AARE genes in Physcomitrella. This gene family expansion is an outstanding feature of the moss family Funariaceae, as most organisms we analysed contain only a single AARE gene, and only a few have two. We analysed those three isoforms in Physcomitrella and compared selected features to the single isoform in Arabidopsis. Our data reveal specific functions in age-related developmental transitions and life span determination.

Surprisingly, we found triple localization of AtAARE and PpAARE1 to chloroplasts, mitochondria and the cytosol *in vivo*, suggesting a functional role for AARE in these cellular compartments. In Physcomitrella, the triple localization is mediated *via* alternative splice variants and in Arabidopsis likely *via* alternative translation initiation. Although there have been indications of AtAARE being associated to chloroplasts (Yamauchi et al., 2003; Nakai et al., 2012), there was no clear evidence for organellar targeting of this protease until now. It is remarkable, that the triple localization of AARE is evolutionary conserved between Arabidopsis and Physcomitrella, although executed *via*

different molecular mechanisms. This suggests an essential and evolutionary conserved function of AARE activity in the cytoplasm, chloroplasts and mitochondria.

Previously, AARE exopeptidase activity was observed in cucumber chloroplasts (Yamauchi et al., 2003), and AARE peptides found in proteomes of Arabidopsis chloroplasts (Zybailov et al., 2008) and mitochondria (Rugen et al., 2021). In contrast, AARE was not identified in plastid or mitochondrial proteomes of Physcomitrella (Mueller et al., 2014; Fesenko et al., 2016). Here, we found AARE exopeptidase activity in chloroplasts and mitochondria of this moss. Chloroplasts are a major source of ROS in photosynthetic tissues exposed to light, whereas mitochondria are the major source of ROS in non-photosynthetic tissues or in the dark (Maxwell et al., 1999; Møller 2001; Noctor et al., 2002, Foyer & Noctor, 2003). Until now, it remained unresolved how plants deplete oxidized proteins from these organelles.

In yeast and mammals, the ATP-dependent LON and AAA proteases are involved in clearance of misfolded and oxidized mitochondrial proteins. Intriguingly, mutants of plant homologs of LON proteases did not show clear effects on the levels of oxidized proteins, but AAA-type FTSH proteases may play a role (reviewed in Smakowska et al., 2014). Nevertheless, stressors such as heat, drought or high light compromise photosynthesis (Al-Khatib & Paulsen, 1989; Wang et al., 2018) and mitochondrial respiration (Sweetlove et al., 2002), leading to a depletion of ATP and to mitochondrial dysfunction (Tiwari et al., 2002). In turn, energy supply for ATP-dependent defence systems such as heat-shock proteins and AAA-type proteases is severely compromised, leaving the question unanswered how oxidized proteins in chloroplasts and mitochondria can be cleared. Because AARE is an ATP-independent protease, our data suggest that organellar-targeted AARE may act as ATP-independent defence to prevent or attenuate protein aggregation in the major ROS-producing organelles.

Based on localization prediction, 70% of our selected plant species possess one AARE isoform that localizes to either plastids or to mitochondria. Whether dual targeting *via* ambiguous targeting also occurs in these species remains to be experimentally validated. Further, we do not exclude that the remaining species also have organellar AARE isoforms, because our predictions may be compromised by incomplete gene models. Such incomplete AARE gene models without a transit peptide were present in earlier genome annotations of Arabidopsis and Physcomitrella (Lamesch et al., 2012; Zimmer et al., 2013), whilst complete gene models with transit peptides were only introduced with later versions (Cheng et al., 2017; Lang et al., 2018).

It is not yet clear how translation of both variants in Arabidopsis is regulated, but a recent study highlights the importance of alternative translation initiation in shaping different subcellular localizations or functions of proteoforms (Willems et al., 2021). This mechanism is also present in Physcomitrella, where dual targeting of FtsZ isoforms to the cytoplasm and chloroplasts is enabled *via* alternative translation initiation (Kiessling et al., 2004). Thus, localization of PpAARE1 to the cytoplasm is also possible from the longer splice variant. Alternative translation initiation of AtAARE is further evidenced by proteomics data (www.peptideatlas.org/builds/arabidopsis/, van Wijk et al., 2021). Here, we found evidence for N-terminal acetylation of M^{56} which is the initiator methionine of the short variant (e.g., Zhang et al., 2019; PXD012708).

Nakai et al. (2012) used the shorter AtAARE ORF and observed the reporter fusion in the cytoplasm and in the nucleus. We did not detect a nuclear localization of any AARE isoform. Using *LOCALIZER* (Sperschneider et al., 2017) we identified an NLS in AtAARE, in PpAARE1 and PpAARE3, but not in PpAARE2. In contrast, the human AARE homolog HsACPH does not have a predictable NLS, but nuclear import is mediated *via* interaction with XRCC1 under stress, where it acts in DNA-damage repair (Zeng et al., 2017). Similarly, a nuclear localization of AARE might occur under stress also *in planta*.

In Physcomitrella, AARE1 is the dominant exopeptidase, whereas AARE2 acts predominantly as endopeptidase, while the operation mode of AARE3 remains unresolved. Crystal structures from bacterial and archaeal AAREs revealed two possible entrances for substrates to the catalytic centres (Bartlam et al., 2004; Brocca et al., 2016) but the mode of substrate entry is not fully understood. Although the quaternary arrangements of subunits differ between species (Menyhárd et al., 2013; Brocca et al., 2016), the secondary structure arrangement is conserved across kingdoms and specific subunit interactions (multimerization) are likely a mechanism to mediate substrate specificity and to modulate activity. This could be further used as a switch between endopeptidase and exopeptidase activity and additionally enable access of the catalytic centre *via* structural re-arrangements. Accordingly, the interaction between the distinct PpAARE isoforms may modify substrate specificity and activity.

Our data indicate a partial compensation between PpAARE1 and PpAARE2. Both single KO mutants are phenotypically inconspicuous under normal conditions, although a significant reduction in the exopeptidase activity was observed in ΔPpAARE1. PpAARE2 had the strongest effect on the accumulation of oxidized proteins in gametophores on the single isoform KO level, whereas the double KO of PpAARE1 and PpAARE2 showed the most striking effect in all lines as accelerated transition from protonema to gametophores. This phenotype is similar to mutants

with perturbed auxin transport (Viaene et al., 2014). However, colony growth in these mutants was reduced which is different from our double KO mutant (PpAARE1/2). Intriguingly, this double KO results in stunted gametophores and a reduced life span. This phenotype partially resembles a loss-of-function mutant of a central component of autophagy (PpATG3) in Physcomitrella (Chen et al., 2020). In ∆PpATG3, gametophores exhibit a reduced life span and colonies are smaller than in WT. In contrast, gametophore size was not affected. Further, photosynthetic capacity in ∆PpATG3 was also reduced, an effect which is apparently not caused by AARE depletion (Nakai et al., 2012) and PpAARE genes were not differentially expressed in ∆PpATG3 (Chen et al., 2020). Thus, we conclude that the reduced life span observed in ∆PpAARE1/2 and ∆PpAARE1/3/2 is not due to an impaired autophagy system causing nitrogen starvation. This is in line with data which opposes autophagy at the onset of senescence in Arabidopsis (Jia et al., 2019).

In mammals, elevated levels of oxidized proteins are associated with age-related pathologies, such as Alzheimer´s disease, diabetes and different types of carcinomas (Dalle-Donne et al., 2003). If proteolytic clearance fails, further accumulation of oxidized proteins causes protein aggregation, which is a hallmark of ageing in animals (López-Otín et al., 2013; Hipp et al. 2019; Chen et al., 2022). A connection between protein oxidation and ageing was less well studied in plants. Plastid ROS levels increase during ageing (Munné-Bosch & Alegre, 2002), which is in line with strong oxidation of plastid proteins in ageing leaves (Johansson et al., 2004). Likewise, protein oxidation marks the developmental transition between vegetative growth and flowering in Arabidopsis (Johansson et al., 2004). Here, we found in Physcomitrella mutants ∆PpAARE1/2 and ∆PpAARE1/3/2 accelerated developmental transition from protonema to gametophores, reduced life span and increased levels of oxidized proteins as signs of accelerated ageing. This is supported by the fact that gametophore tips, which is younger tissue, are longer viable than the older stems in both mutants. In the Arabidopsis AARE T-DNA mutants we found increased levels of oxidized proteins under normal cultivation conditions and an accelerated developmental transition, in this case premature bolting. These findings suggest an evolutionary conserved connection between protein oxidation and ageing.

Age-related developmental transitions in plants such as meristem formation by time-resolved action of micro RNAs and hormonal crosstalk are well studied (Laufs et al., 2004; Wu & Poethig, 2006; Yant et al., 2010; Arif et al., 2012; Singh et al., 2014; reviewed in Rankenberg et al., 2021). Induction of bolting and flowering is tightly linked to temperature (Balasubramanian et al., 2006) but independent of day length (Wei et al., 2017). The transition from the vegetative to the

reproductive phase is mediated *via* transcriptional regulation of FLOWERING LOCUS M (FLM) and SHORT VEGETATIVE PHASE (SVP, Lee et al., 2013; Posé et al., 2013). Central components of the transcriptional regulation of FLM are splicing factor 1 (Lee et al., 2020) and the ribonucleoprotein RBP45d (Chang et al., 2022). However, it is not yet fully resolved how temperature sensing is finally transmitted to cause transcriptional regulation in progressive ageing. Based on our data, we suggest protein oxidation as a missing link between temperature sensing and regulation of ageing in plants. In turn, AARE activity reduces stress-related levels of oxidized proteins and thus delays ageing and related developmental transitions from the vegetative to the generative phase in plants.

We here provide a detailed analysis of AARE genes in the plant lineage and an in-depth analysis of AARE localization and function in the moss Physcomitrella and the angiosperm Arabidopsis. AARE loss-of-function mutants have not been described for any organism so far. We generated and analysed such mutants and describe a connection between AARE function, aggregation of oxidized proteins and plant ageing, including accelerated developmental progression and reduced life span. Our findings complement similar findings in humans and animals where AARE malfunction is associated with protein aggregation and age-related pathologies. Together, these findings can support a unified concept of ageing in different life forms.

Methods

Cultivation of Physcomitrella

Physcomitrella WT (new species name: *Physcomitrium patens* (Hedw.) Mitt.; Medina et al. (2019)), ecotype “Gransden 2004” and AARE KO lines were cultivated in Knop medium supplemented with microelements. Knop medium (pH 5.8) containing 250 mg/L KH_2PO_4, 250 mg/L KCl, 250 mg/L $MgSO_4$ x 7 H_2O, 1,000 mg/L $Ca(NO_3)_2$ x 4 H_2O and 12.5 mg/L $FeSO_4$ x 7 H_2O was prepared as described in Reski and Abel (1985) and supplemented with 10 mL per liter of a microelement (ME) stock solution (309 mg/L H_3BO_3, 845 mg/L $MnSO_4$ x 1 H_2O, 431 mg/L $ZnSO_4$ x 7 H_2O, 41.5 mg/L KI, 12.1 mg/L Na_2MoO_4 x 2 H_2O, 1.25 mg/L $CoSO_4$ x 5 H_2O, 1.46 mg/L $Co(NO_3)_2$ x 6 H_2O) as described by Egener et al. (2002) and Schween et al. (2003). For cultivation on solid medium, 12 g/L Agar was added to the KnopME medium. Moss suspension cultures were disrupted weekly with an ULTRA-TURRAX (IKA) at 18,000 rpm for 90 s. If not indicated otherwise, moss was grown under standard light conditions (55 µmol photons/m^2s) at 22°C in a 16h/8h light/dark cycle.

Hydroponic Physcomitrella gametophore cultures were as described in Erxleben et al. (2012) and Hoernstein et al. (2016). In brief, a thin layer of protonema from suspension was spotted on gauze mesh (PP, 250 m mesh, 215 m thread, Zitt Thoma GmbH, Freiburg, Germany) capped on a glass ring. The glass rings with protonema-covered mesh gauze were placed in Magenta®Vessels (Sigma-Aldrich, St. Louis, USA) and KnopME medium was added until the protonema-covered gauze mesh was moist. The medium was exchanged every 4 weeks. Gametophores were harvested after 12 weeks.

Gametophore colonies on Agar plates (KnopME) were generated by transplanting single gametophores to new plates. Plates were sealed with Parafilm®.

Generation of AARE knockout lines

Knockout constructs for each AARE gene were generated by amplifying genomic regions as homologous flanks. The PCR products were fused to a neomycin (AARE1), hygromycin (AARE2) and zeocin (AARE3) resistance cassettes, respectively, employing triple template PCR described in Tian et al. (2004) with primer sequences listed in Table S1f using the *Q5* polymerase (New England Biolabs, Ipswich, USA). The knockout constructs were released from their vector backbones with XhoI (PpAARE1), BglII (PpAARE2) and DraI (PpAARE3), respectively. Enzymes were purchased from Thermo Fisher Scientific. Digested plasmids were precipitated and sterilized prior to transfection using standard ethanol precipitation method (Sambrook & Russell, 2006). Transfection of Physcomitrella WT or KO (for consecutive knockouts) protoplasts was conducted as described (Hohe & Reski, 2002; Hohe et al., 2004). The WT strain as well as the identified PpAARE KO lines are accessible via the International Moss Stock Center (IMSC, www.moss-stock-center.org). IMSC accession numbers for the mutant and WT are available in Table S4.

Screening of plants surviving antibiotics selection was done by PCR. KO mutant plants surviving the antibiotics selection were checked for the presence of a genomic region which should be removed upon homologous recombination-based integration of the knockout construct (Fig. S4a). In case of the absence of this WT signal, plants were further checked for correct 5' and 3' integration of the respective knockout construct using primers listed in Table S1.

Protonema growth and gametophore induction

Suspension cultures were started at the same day and disrupted weekly as described. Dry weight was measured in triplicates and suspension density was adjusted to 440 mg/mL as described in Decker et al. (2017). Droplets of 15 µL were spotted on solid medium (Knop ME, 0.02% glucose).

Sealed plates were cultivated as described above. Each three droplets per line were spotted on one plate and all lines were spotted on the same plate. 3 plates (12 colonies) were used per assay. Colony areas were measured with *ImageJ*. White pixels counted from binarized colony images were used as quantitative values. Gametophores were counted upon visibility of the first leafy structure on buds.

Generation of PpAARE-Citrine knock-in lines

Knock-in constructs to fuse the coding sequence of Citrine to the C-terminus of PpAARE isoforms via an 18 bp linker (Tian et al., 2004) at the endogenous genomic locus were cloned via Gibson assembly as described (Gibson et al., 2009). All necessary parts were amplified using primers listed in Table S1. Additionally, XhoI (PpAARE1), SalI (PpAARE2) and BamHI (PpAARE3) restriction sites were added to the 5' and the 3' ends of the respective knock-in construct. All parts were assembled into pJet1.2 vector backbone (Thermo Scientific) using the Gibson Assembly®Cloning Kit from New England Biolabs (Ipswich, Massachusetts, USA). Transfection of Physcomitrella WT protoplasts were conducted as described (Hohe & Reski, 2002; Hohe et al., 2004) by co-transfecting a plasmid containing a neomycin phosphotransferase resistance (nptII) cassette as transient selection marker (pBSNNNEV, Mueller et al., 2014). The linearized plasmid and the co-transfection vector were purified and sterilized *via* ethanol precipitation (Sambrook & Russell, 2006) prior to transfection.

The presence of Citrine was checked with primers listed in Table S1 and resulting positive lines were further checked for correct 5' and 3' integration by PCR using the Plant Phire Kit with primers listed in Table S1. All identified fusion lines are available *via* the International Moss Stock Center (IMSC, www.moss-stock-center.org). IMSC accessions are listed in Table S4.

qPCR analysis

The copy number of the integrated KO constructs was determined using a qPCR-based method as described in Noy-Malka et al. (2014). Genomic DNA was extracted from 100 mg frozen protonema using the GeneJEt Plant Genomic DNA Purification Kit (Thermo Scientific, Waltham, USA). DNA concentrations were adjusted to 3 ng/µl for each sample and qPCR was performed with primers for the 5' and the 3' flanks as well as with primers for the corresponding selection cassette. Additionally, primers for the single copy gene CLF (Pp3c22_2940V3) were used as internal control. Reference lines were WT as well as in-house lines with known single integrations of the used selection cassettes. Primers are listed in Table S5. PCR reactions were done using

2x SensiFAST Mix (Bioline, London, UK) and analyzed in a Lightcycler 480 II (Roche, Basel, Schweiz).

cDNA preparation

RNA was extracted using the innuPREP Plant RNA Kit (Analytik Jena, Jena, Germany). The extracted RNA was treated with DNAse I (Thermo Scientific) and subsequently reverse transcribed into cDNA using Superscript III Reverse Transcriptase (Life Technologies, Carlsbad, USA).

Fusion constructs for subcellular localization

All constructs were generated using Gibson assembly and integrated into a PpAct5:Linker:eGFP-MAV4 vector backbone described in Özdemir et al. (2018). Integration of the different coding sequences was done in frame in front of the Linker:eGFP. All parts for the Gibson assembly (inserts and corresponding vector backbones) were amplified either with Phusion™ polymerase (Thermo Fisher Scientific) or with HiFi polymerase (PCR Biosystems Ltd) according to the manufacturer´s instructions. The primers were designed to have a 25 bp overlap to the corresponding fragment to be fused with. All primers and combinations are listed in Table S6. In the case of the N-terminal difference of AtAARE (M^1-A^{55} of AT4G14570.1, gene model provided by TAIR (https://www.arabidopsis.org/)) the Actin5 promotor was replaced by the CaMV35S promotor (Amack & Antunes, 2020) previously validated in Physcomitrella (Horstmann et al., 2004).

Cloned plasmids were purified using the PureYield™ Plasmid Midiprep kit (Promega, Wisconsin, USA) according to the manufacturer´s instructions. The plasmids were purified and sterilized *via* ethanol precipitation (Sambrook & Russell, 2006).

Confocal microscopy

Confocal imaging was performed on transiently transfected live protoplasts using Leica TCS SP8 (Leica Microsystems, Wetzlar, Germany). Immediately before microscopy, MitoTracker™ Orange CMTMRos (ThermoFisher Scientific) was added to protoplast suspensions to a final concentration of 100 nM. For all imaging experiments, an HC PL APO CS2 63x/1.40 OIL objective was used with a zoom factor of 4. The pinhole was set to 35.4 µm. For excitation, a WLL laser (70%) was used. In a sequential acquisition setup, eGFP and chlorophyll were excited with the same laser beam (488 nm, 2%) and their signals were detected simultaneously, whereas MitoTracker™ was excited with a different laser beam (550 nm, 2%) and its signal was detected separately. The

detection ranges were specified as 502 nm - 546 nm for eGFP, 662 nm - 732 nm for chlorophyll and 597 nm - 636 nm for MitoTracker™. The images were acquired as z-stacks with the number of optical sections varying with the protoplast size. The voxel sizes of the resulting z-stacks were 0.0903, 0.0903, 0.239 µm in the x-y-z order. For visual representation and analysis, single slices with the best signal-to-noise ratio were selected and extracted from each z-stack using FIJI software.

Cultivation of Arabidopsis

Seeds were surface-sterilized for 4 min in 80% ethanol and subsequently for 1 min in 100% ethanol. Seeds were placed on plates containing ½ MS supplemented with 1% (D+) sucrose and 0.8% Agar. Alternatively, seeds were directly placed on sterilized soil. Seeds were incubated at 8°C for 2-4 days in the dark for stratification before placing them in growth chambers. Plants were further cultivated under short day conditions at 22°C and 70 µmol photons/m^2s in an 8h/16h light/dark cycle. For bolting assays, plants were placed in a phyto-chamber at 22°C and 70 µmol photons/m^2s in a 16h/8h light/dark cycle (long day condition). Rosette leaves and days since sowing were counted upon appearance of the shoot in the middle of the rosette.

Screening of Arabidopsis AARE mutants

Arabidopsis thaliana lines with T-DNA insertions in the At4G14570 locus were identified from the public T-DNA Express database at the SIGnAL website (Salk Institute Genomic Analysis Laboratory). Lines GK-456A10, SALK_080653C, SALK_071125C, and SALK_205137C, were obtained from the Nottingham Arabidopsis Stock Centre. Homozygous mutant alleles were verified by PCR using the following primers: forward LB GK 5´-ATATTGACCATCATACTCATTGC-3´ and reverse GK-456 5´-CTTCAAAGAAACACCAATCAG-3´for the GK-456A10 line, and forward LB-pROK 5´-GCGTGGACCGCTTGCTGCAACT-3´ and reverse Salk_53 5´-TCTTTAGCCGAATCAGTTCCAGA-3´for the SALK_080653C, SALK_071125C, and SALK_205137C lines. Identified homozygous mutant plants were back-crossed with Arabidopsis Col-0. The F2 generation was screened for homozygous mutant plants using the above listed primer-sets to identify the mutant allele or substituting the forward primers with forward WT-GK-456 5´-AAGATGCTTTGCAGTCTCTA-3´ and forward WT-Salk 5´-ACTGCCTTATGATCCATTGTCTC-3´, to identify the GK and SALK lines WT alleles, respectively. RT-PCR was additionally performed to check for the presence of AtAARE transcripts using Taq polymerase on cDNA prepared as described above with primers At1-At4. All primer combinations are listed in Table S4.

AARE exopeptidase activity

The enzyme activity assay of Yamauchi et al. (2003) was modified. In brief, tissue (80-100 mg) was homogenized in liquid nitrogen and dissolved in 1 mL extraction buffer (50 mM PBS, 1 mM EDTA, 2 mM DTT). After centrifugation at 20,000 x g for 20 min at 4°C, 300 µl supernatant was mixed with 700 µL reaction buffer (50 mM HEPES-KOH, pH 7.5 containing 1 mM Ac-Ala-pNA (Bachem, Bubendorf, Switzerland) or 50 mM HEPES-KOH, pH 7.5, 10% DMSO containing 1mM AcLeu-pNA (Bachem) and incubated at 37°C for 30-120 min. The reaction was stopped by the addition of 500 µL 30% acetic acid. Absorbance was measured at 410 nm in a photospectrometer. This approach was used to generate the data of Fig. 3b and Fig. S6a-d. Later the method was modified (Fig. 3g, Fig. S6e-g). Here, tissue was homogenized in liquid nitrogen and dissolved in 100 µL extraction buffer (50 mM PBS, 1 mM EDTA, 2 mM DTT) per 10 mg FW. After centrifugation at 20,000 x g for 20 min at 4°C, 5 µl supernatant was mixed with 195 µL reaction buffer (50 mM HEPES-KOH, pH 7.5 containing 1 mM Ac-Ala-pNA (Bachem, Bubendorf, Switzerland)) in a 96 well micro titer plate and incubated at 37°C for 30-120 min. In the case of Ac-Leu-pNA as substrate, 50 mM HEPES-KOH, pH 7.5 with 10% DMSO containing 1mM AcLeu-pNA (Bachem) was used as reaction buffer. Every biological sample was measured in three technical replicates. Absorbance was measured at 410 nm. Activity was calculated using a molar absorbance coefficient of 8.8 $mM*cm^{-1}$ according to Nakai et al. (2012) and represents the release of pNA [µmol] per minute normalized to the total protein concentration of the sample. The protein concentration was determined using the A_{280} method of a NanoDrop™ (Thermo Fisher Scientific) or with a Bradford assay (Bradford, 1976).

Western Blot

Western Blots were performed as described in Lang et al. (2011) using the *ECL Advance detection kit* (GE Healthcare). The primary antibody against *A. thaliana* AARE was kindly provided by Dr. Yasuo Yamauchi and is described in Yamauchi et al. (2003). The primary antibody was diluted 1:10,000 in TBST-Buffer with 2% Blocking (GE Healthcare) and incubated on the membrane for 2 h. As secondary antibody anti-Guinea pig antibody, coupled to a horseradish peroxidase (Agrisera, AS 10 1496) diluted 1:10,000 in 2% TBST with 2% Blocking (GE Healthcare), was applied for 1 h.

Detection of oxidized proteins

Plant tissues were homogenized in liquid nitrogen and proteins were extracted in 50 mM PBS, 50 mM DTT, 1 mM EDTA. 3-6 µg total protein was derivatized with DNPH and subsequently detected

with an anti-DNP antibody according to the manufacturer's instruction of the *OxyBlot Protein Oxidation Detectio*n Kit (S7150, Sigma-Aldrich). Equal amounts of the derivatized protein samples were employed as loading control on a separate SDS-gel and stained with Coomassie or silver staining.

Flow cytometry

FCM analysis was performed according to Heck et al. (2021). In brief, protonemata were chopped with a razor blade in a small petri dish (6 cm diameter) in 2 mL of DAPI-buffer containing 0.01 mg/L 4′,6-Diamidin-2-phenylindol (DAPI), 1.07 g/L $MgCl_2$ x 6 H_2O, 5 g/L NaCl, 21.11g/L Tris, 0.1% Triton, pH 7. The solution was filtered using 30 µm pore size filters and the fluorescence intensity was measured using a Cyflow®Space flow cytometry system (Partec, Munich, Germany).

Computational predictions

Predictions for the presence of cleavable targeting peptides were performed with *TargetP2.0* (Armenteros et al., 2019). Additional predictions of subcellular localizations were performed with *LOCALIZER* (Sperschneider et al., 2017). The presence of peroxisomal targeting signals was predicted with *PredPlantPTS1* (Lingner et al., 2011; Reumann et al., 2012). Prediction of protein domains was performed using *InterProScan* (Blum et al., 2021) and protein domain annotations according to PFAM (Mistry et al., 2021) were used.

Co-Immunoprecipitation

Co-immunoprecipitation was performed using GFP-Trap Magnetic Particles M-270 (Chromotek, Planegg-Martinsried, Germany) as recommended by the manufacturer with modifications. 300 mg protonema was homogenized in a 2 mL reaction tube using a tungsten and a glass bead. For each line three biological replicates were realized. The extraction buffer was chosen according to the manufacturer's recommendations for plant samples and contained 25 mM HEPES-KOH, pH7.5, 2 mM EDTA, 100 mM NaCl, 200 nM DTT, 0.5% Triton X-100, 1% plant protease inhibitor cocktail (PPI, P9599, Sigma Aldrich). Ground plant material was dissolved in a final volume of 2 mL ice-cold extraction buffer and incubated for 10 min in a water quench ultrasonic device. Samples were centrifuged at 4°C at 20,000xg for 30 min. For each sample 25 µL magnetic particle slurry was washed with 500 µL extraction buffer. The sample supernatant was transferred to the cleaned beads and incubated, rotating for 1 h at 6°C. Subsequently, beads were washed with 1 mL extraction buffer without Triton and PPI and again with 500 µL. Beads were then dissolved in 500 µL wash buffer (10 mM Tris-HCl, pH7.5, 150 mM NaCl, 0.5 mM EDTA), transferred to a new

reaction tube and washed again in 500 µL wash buffer. A RapiGest solution (0.2% in 50 mM Tris-HCl, pH7.5; RapiGest SF Surfactant (Waters, Milford, MA, USA) was mixed 3:1 with 5 mM DTT in 50 mM Tris-HCl, pH7.5. 30 µL of the resulting mixture were applied on each sample. Samples were incubated at 95°C for 5 min under continuous shaking. Samples were cooled down to RT and 5 µL of a trypsin (V5117, P) solution (0.025 µg/µL in 50 mM Tris-HCl, pH 7.5) were added to each sample. Digestion on the beads was performed for 30 min at 32°C under continuous shaking. Supernatants were transferred to new reaction tubes and the remaining beads were washed twice with 50 µL 5 mM Iodoacetamide solution (in 50 mM Tris-HCl, pH7.5). The wash supernatants were combined with the trypsin-containing supernatant and incubated over night at 30°C under continuous shaking. Acid-catalysed cleavage of the RapiGest surfactant was performed as recommended by the manufacturer. Samples were purified using C18-STAGE-Tips as described in Hoernstein et al. (2018) and eluted from the Tip in 30% ACN in 0.1% FA.

Mass spectrometry measurement and data analysis

MS analysis was performed on an Orbitrap Q-Exactive Plus instrument (Thermo Fisher Scientific) coupled to an UltiMate 3000 RSLCnano system (Dionex LC Packings/Thermo Fisher Scientific) as described in Top et al. (2021). Database search and label-free quantitation was performed using *MaxQuant* software V 1.6.0.16 (Cox & Mann, 2008) as described in Hoernstein et al. (2016). For each Co-IP a specific database was employed containing all V3.3 proteins of Physcomitrella (Lang et al., 2018) as well as the sequence of the fusion protein. Additionally, the contaminant list provided by the software was included. Decoys were generated on the fly by reverting the given protein sequences. Variable modifications were formation of pyro Glu (N term Q, −17.026549 Da), oxidation (M, +15.994915 Da), acetylation (N-term, +42.010565 Da) and deamidation (N, +0.9 84016 Da). Carbamidomethylation (C, +57. 021464 Da) was specified as fixed modification. Enzymatic specificity was set to tryptic with semi-specific free N-terminus. An FDR of 0.01 was set for protein identification. LFQ values (Cox et al., 2014) were used as quantitative values. Interaction analysis was performed in Perseus V 1.6.12.0 (Tyanova et al., 2016). Missing values were imputed from a normal distribution with a down-shift of 1.8 and distribution width of 0.3. Interaction partners were accepted at an FDR of 0.01 and a p-value less than 0.01.

Processed mgf files from immunoprecipitation experiments targeting N-terminal arginylation (Hoernstein et al., 2016, PXD003232) were searched again against all Physcomitrella protein models V3.3 (Lang et al., 2018) using Mascot Server V2.7.0 (Matrix Science). The precursor mass tolerance was 5 ppm and the fragment mass tolerance was 0.02 Da. Variable modifications were formation of pyro Glu (N term Q, −17.026549 Da), oxidation (M, +15.994915 Da), acetylation (N-

term, +42.010565 Da) and deamidation (N, +0.9 84016 Da). Carbamidomethylation (C, +57. 021464 Da) was specified as fixed modification. Enzymatic specificity was set to tryptic with semi-specific free N-terminus. Search results were loaded in Scaffold™ 5 (V5.0.1, Proteome Software) and proteins were accepted at an FDR = 1 and peptides at an FDR = 0.5. A table of identified proteins is accessible in Table S7.

Multiple sequence alignment and phylogenetic reconstruction

Homologous protein sequences were aligned with UPP (version 4.4.0; Nguyen et al., 2015) using default parameters and subsequently translated into a codon-aware CDS alignment with PAL2NAL (version 1.4; Suyama et al., 2006). Based on this multiple coding sequence alignment we reconstructed a maximum likelihood tree with RAxML (version 8.2.12; Stamatakis, 2014) using the GTRCAT model with 1000 rapid bootstrap samples. The tree was rooted at the split between animal and plant sequences and plotted in R (R Core Team, 2022) using the packages ape (Paradis & Schliep, 2018) and ggtree (Yu et al., 2017).

Data availability

The authors confirm that all relevant data supporting the findings of this study are available within the paper and its supplementary files. The mass spectrometry proteomics data have been deposited at the ProteomeXchange Consortium via the PRIDE partner repository (Deutsch et al., 2020; Perez-Riverol et al., 2022) with the dataset identifier PXD033854. Plant lines used in this study are available upon request from the corresponding author (R.R.).

Acknowledgements

We thank Christine Glockner, Agnes Novakovic and Eija Schulze for expert technical assistance and Anne Katrin Prowse for language editing. Support with the Arabidopsis assays from Dr. Philipp Schwenk is gratefully acknowledged. We thank Prof. Dr. Bettina Warscheid for the possibility to use the QExactive Plus instrument and Prof. Dr. Yasuo Yamauchi for the primary antibody against *A. thaliana* AARE. We gratefully acknowledge funding by the Deutsche Forschungsgemeinschaft (DFG, German Research Foundation) under Germany's Excellence Strategy EXC-2189 (CIBSS to R.R.) and by the Wissenschaftliche Gesellschaft Freiburg.

Author contributions

S.N.W.H. designed research, performed experiments, analysed data, and wrote the manuscript. B.Ö. and N.v.G. analysed data and helped writing the manuscript. A.A.M. analysed data. B.R.v.B., L.N., J.S.F., R.K., S.G., T.W., and F.S. performed experiments. M.R.F. and S.J.M.S. designed research and helped writing the manuscript. R.R. designed and supervised research, acquired funding, and wrote the manuscript. All authors approved the final version of the manuscript.

Funding

Open Access funding enabled and organized by Projekt DEAL.

Competing interests

All authors declare to have no competing interests.

References

Al-Khatib K, Paulsen GM (1989) Enhancement of thermal injury to photosynthesis in wheat plants and thylakoids by high light intensity. *Plant Physiology* 90: 1041-1048

Altschul SF, Madden TL, Schäffer AA, Zhang J, Zhang Z, Miller W, Lipman DJ (1997) Gapped BLAST and PSI-BLAST: a new generation of protein database search programs. *Nucleic Acids Research* 25: 3389-3402

Amack SC, Antunes MS (2020) CaMV35S promoter–a plant biology and biotechnology workhorse in the era of synthetic biology. *Current Plant Biology* 24: 100179

Arif MA, Fattash I, Ma ZR, Cho SH, Beike AK, Reski R, Axtell MJ, Frank W (2012) DICER-LIKE3 activity in *Physcomitrella patens* DICER-LIKE4 mutants cause severe developmental dysfunction and sterility. *Molecular Plant* 6: 1281-1294

Armenteros JJA, Salvatore M, Emanuelsson O, Winther O, von Heijne G, Elofsson A, Nielsen H (2019) Detecting sequence signals in targeting peptides using deep learning. *Life Science Alliance* 2: e201900429

Ashton NW, Grimsley NH, Cove DJ (1979) Analysis of gametophytic development in the moss, *Physcomitrella patens*, using auxin and cytokinin resistant mutants. *Planta* 144: 427-435.

Bachovchin DA, Koblan LW, Wu W, Liu Y, Li Y, et al. (2014) A high-throughput, multiplexed assay for superfamily-wide profiling of enzyme activity. *Nature Chemical Biology*, 10: 656-663.

Balasubramanian S, Sureshkumar S, Lempe J, Weigel D (2006) Potent induction of *Arabidopsis thaliana* flowering by elevated growth temperature. *PLOS GENETICS* 2: e106

Banks JA, Nishiyama T, Hasebe M, Bowman JL, Gribskov M, DePamphilis C, et al. (2011) The *Selaginella* genome identifies genetic changes associated with the evolution of vascular plants. *Science* 332: 960-963

Bartlam M, Wang G, Yang H, Gao R, Zhao X, Xie G, et al. (2004) Crystal structure of an acylpeptide hydrolase/esterase from *Aeropyrum pernix K1*. *Structure* 12: 1481-1488

Bergamo P, Cocca E, Palumbo R, Gogliettino M, Rossi M, Palmieri G (2013) RedOx status, proteasome and APEH: Insights into anticancer mechanisms of t10, c12-conjugated linoleic acid isomer on A375 melanoma cells. *PLOS ONE* 8: e80900

Blum M, Chang HY, Chuguransky S, Grego T, Kandasaamy S, Mitchell A, et al. (2021) The InterPro protein families and domains database: 20 years on. *Nucleic Acids Research* 49: D344-D354

Bowman JL, Kohchi T, Yamato KT, Jenkins J, Shu S, Ishizaki K, et al. (2017) Insights into land plant evolution garnered from the *Marchantia polymorpha* genome. *Cell* 171: 287-304

Bradford MM (1976) A rapid and sensitive method for the quantitation of microgram quantities of protein utilizing the principle of protein-dye binding. *Analytical Biochemistry* 72: 248-254

Brocca S, Ferrari C, Barbiroli A, Pesce A, Lotti M, Nardini M. (2016) A bacterial acyl aminoacyl peptidase couples flexibility and stability as a result of cold adaptation. *FEBS Journal* 283: 4310-4324

Brunialti EA, Gatti-Lafranconi P, Lotti M (2011) Promiscuity, stability and cold adaptation of a newly isolated acylaminoacyl peptidase. *Biochimie* 93: 1543-1554

Chang P, Hsieh HY, Tu SL (2022) The U1 snRNP component RBP45d regulates temperature-responsive flowering in Arabidopsis. *Plant Cell* 34: 834-851

Chen F, Mackey AJ, Stoeckert Jr CJ, Roos DS (2006) OrthoMCL-DB: querying a comprehensive multi-species collection of ortholog groups. *Nucleic Acids Research* 34: D363-D368

Chen YR, Harel I, Singh PP, Zviv I, Moses E, Goshtchevsky U, Machado BE, Brunet A, Jarosz DF (2022) Tissue-specific landscape of protein aggregation and quality control in an aging vertebrate. *bioRxiv*: https://doi.org/10.1101/2022.02.26.482120

Chen Z, Wang W, Pu X, Dong X, Gao B, Li P, et al. (2020) Comprehensive analysis of the Ppatg3 mutant reveals that autophagy plays important roles in gametophore senescence in *Physcomitrella patens*. *BMC Plant Biology* 20: 440

Cheng CY, Krishnakumar V, Chan AP, Thibaud-Nissen F, Schobel S, Town CD (2017) Araport11: a complete reannotation of the *Arabidopsis thaliana* reference genome. *Plant Journal* 89: 789-804

Ciacka K, Tymiński M, Gniazdowska A, Krasuska U (2020) Carbonylation of proteins—an element of plant ageing. *Planta* 252: 12

Cox J, Mann M (2008) MaxQuant enables high peptide identification rates, individualized ppb-range mass accuracies and proteome-wide protein quantification. *Nature Biotechnology* 26: 1367-1372

Cox J, Hein MY, Luber CA, Paron I, Nagaraj N, Mann M (2014) Accurate proteome-wide label-free quantification by delayed normalization and maximal peptide ratio extraction, termed MaxLFQ. *Molecular & Cellular Proteomics* 13: 2513-2526

Dalle-Donne I, Giustarini D, Colombo R, Rossi R, Milzani A (2003) Protein carbonylation in human diseases. *Trends in Molecular Medicine* 9: 169-176

Dalle-Donne I, Carini M, Orioli M, Vistoli G, Regazzoni L, Colombo G, et al. (2009) Protein carbonylation: 2, 4-dinitrophenylhydrazine reacts with both aldehydes/ketones and sulfenic acids. *Free Radical Biology and Medicine* 46: 1411-1419

Decker, EL, Alder, A, Hunn, S, Ferguson, J, Lehtonen, MT, Scheler, B, et al. (2017). Strigolactone biosynthesis is evolutionarily conserved, regulated by phosphate starvation and contributes to resistance against phytopathogenic fungi in a moss, *Physcomitrella patens*. *New Phytologist* 216: 455-468.

Deutsch, EW, Bandeira, N, Sharma, V, Perez-Riverol, Y, Carver, JJ, Kundu, DJ, et al. (2020). The ProteomeXchange consortium in 2020: enabling 'big data' approaches in proteomics. *Nucleic Acids Research* 48: D1145-D1152

Egener T, Granado J, Guitton MC, Hohe A, Holtorf H, Lucht JM, et al. (2002) High frequency of phenotypic deviations in *Physcomitrella patens* plants transformed with a gene-disruption library. *BMC Plant Biology* 2: 6

Erxleben A, Gessler A, Vervliet-Scheebaum M, Reski R (2012) Metabolite profiling of the moss *Physcomitrella patens* reveals evolutionary conservation of osmoprotective substances. *Plant Cell Reports* 31: 427-436

Farooq MA, Niazi AK, Akhtar J, Saifullah, Farooq M, Souri Z, Karimi N, Rengel Z (2019) Acquiring control: The evolution of ROS-Induced oxidative stress and redox signaling pathways in plant stress responses. *Plant Physiology and Biochemistry* 141: 353-369

Fernandez-Pozo N, Haas FB, Meyberg R, Ullrich KK, Hiss M, Perroud PF, et al. (2020) PEATmoss (Physcomitrella Expression Atlas Tool): a unified gene expression atlas for the model plant *Physcomitrella patens*. *Plant Journal* 102: 165-177

Fesenko IA, Arapidi GP, Skripnikov AY, Alexeev DG, Kostryukova ES, Manolov AI, et al. (2015) Specific pools of endogenous peptides are present in gametophore, protonema, and protoplast cells of the moss *Physcomitrella patens*. *BMC Plant Biology* 15: 87

Fesenko I, Seredina A, Arapidi G, Ptushenko V, Urban A, Butenko I, et al. (2016) The *Physcomitrella patens* chloroplast proteome changes in response to protoplastation. *Frontiers in Plant Science* 7: 1661

Foyer CH, Noctor G (2003) Redox sensing and signalling associated with reactive oxygen in chloroplasts, peroxisomes and mitochondria. *Physiologia Plantarum* 119: 355-364

Fujino T, Kojima M, Beppu M, Kikugawa K, Yasuda H, Takahashi K (2000) Identification of the cleavage sites of oxidized protein that are susceptible to oxidized protein hydrolase (OPH) in the primary and tertiary structures of the protein. *Journal of Biochemistry* 127: 1087-1093

Fuss J, Liegmann O, Krause K, Rensing SA (2013) Green targeting predictor and ambiguous targeting predictor 2: the pitfalls of plant protein targeting prediction and of transient protein expression in heterologous systems. *New Phytologist* 200: 1022-1033

Gibson DG, Young L, Chuang RY, Venter JC, Hutchison CA, Smith HO (2009) Enzymatic assembly of DNA molecules up to several hundred kilobases. *Nature Methods* 6: 343–345

Giorgi C, Marchi S, Simoes IC, Ren Z, Morciano G, Perrone M, et al. (2018) Mitochondria and reactive oxygen species in aging and age-related diseases. *International Review of Cell and Molecular Biology* 340: 209-344

Gogliettino M, Balestrieri M, Cocca E, Mucerino S, Rossi M, Petrillo M, et al. (2012) Identification and characterisation of a novel acylpeptide hydrolase from *Sulfolobus solfataricus*: structural and functional insights. *PLOS ONE* 7: e37921

Gogliettino M, Riccio A, Balestrieri M, Cocca E, Facchiano A, D'Arco TM, et al. (2014) A novel class of bifunctional acylpeptide hydrolases–potential role in the antioxidant defense systems of the Antarctic fish *Trematomus bernacchii*. *FEBS Journal* 281: 401-415

Gogliettino M, Cocca E, Sandomenico A, Gratino L, Iaccarino E, Calvanese L, et al. (2021) Selective inhibition of acylpeptide hydrolase in SAOS-2 osteosarcoma cells: is this enzyme a viable anticancer target? *Molecular Biology Reports* 48: 1505-1519

Gould SJ, Keller G A, Hosken N, Wilkinson J, Subramani S (1989) A conserved tripeptide sorts proteins to peroxisomes. *Journal of Cell Biology* 108: 1657-1664

Gratão PL, Polle A, Lea PJ, Azevedo RA (2005) Making the life of heavy metal-stressed plants a little easier. *Functional Plant Biology* 32: 481-494

Harman D (1956) Aging: A theory based on free radical and radiation chemistry. *Journal of Gerontology* 11: 298–300

Harman D (1972) The biologic clock: the mitochondria? *Journal of the American Geriatrics Society* 20: 145-147

Heck MA, Lüth VM, van Gessel N, Krebs M, Kohl M, Prager A, Joosten H, Decker EL, Reski R (2021) Axenic *in vitro* cultivation of 19 peat moss (*Sphagnum* L.) species as a resource for basic biology, biotechnology, and paludiculture. *New Phytologist* 229: 861-876

Hipp MS, Kasturi P, Hartl FU (2019) The proteostasis network and its decline in ageing. *Nature Reviews Molecular Cell Biology* 20: 421-435

Hoernstein SNW, Mueller SJ, Fiedler K, Schuelke M, Vanselow JT, Schuessele C, et al. (2016) Identification of targets and interaction partners of arginyl-tRNA protein transferase in the moss *Physcomitrella patens*. *Molecular & Cellular Proteomics* 15: 1808-1822

Hoernstein SNW, Fode B, Wiedemann G, Lang D, Niederkrüger H, Berg B, et al. (2018) Host cell proteome of *Physcomitrella patens* harbors proteases and protease inhibitors under bioproduction conditions. *Journal of Proteome Research* 17: 3749-3760

Hohe A, Reski R (2002) Optimisation of a bioreactor culture of the moss *Physcomitrella patens* for mass production of protoplasts. *Plant Science* 163: 69-74

Hohe A, Egener T, Lucht JM, Holtorf H, Reinhard C, Schween G, Reski R (2004) An improved and highly standardised transformation procedure allows efficient production of single and multiple targeted gene-knockouts in a moss, *Physcomitrella patens*. *Current Genetics* 44: 339-347

Hori K, Maruyama F, Fujisawa T, Togashi T, Yamamoto N, Seo M, et al. (2014) *Klebsormidium flaccidum* genome reveals primary factors for plant terrestrial adaptation. *Nature Communications* 5: 3978

Horstmann V, Huether CM, Jost W, Reski R, Decker EL (2004) Quantitative promoter analysis in *Physcomitrella patens*: a set of plant vectors activating gene expression within three orders of magnitude. *BMC Biotechnology* 4: 13

Jia M, Liu X, Xue H, Shi L, Wang R, Chen Y, et al. (2019) Noncanonical ATG8-ABS3 interaction controls senescence in plants. *Nature Plants* 5: 212-224

Johansson E, Olsson O, Nyström T (2004) Progression and specificity of protein oxidation in the life cycle of *Arabidopsis thaliana*. *Journal of Biological Chemistry* 279: 22204-22208

Kiessling J, Martin A, Gremillon L, Rensing SA, Nick P, Sarnighausen E, et al. (2004) Dual targeting of plastid division protein FtsZ to chloroplasts and the cytoplasm. *EMBO Reports* 5: 889-894

Kirbis A, Waller M, Ricca M, Bont Z, Neubauer A, Goffinet B, Szövényi P (2020) Transcriptional landscapes of divergent sporophyte development in two mosses, *Physcomitrium* (Physcomitrella) *patens* and *Funaria hygrometrica*. *Frontiers in Plant Science* 11: 747

Kiss AL, Hornung B, Rádi K, Gengeliczki Z, Sztáray B, Juhász T, et al. (2007) The acylaminoacyl peptidase from *Aeropyrum pernix* K1 thought to be an exopeptidase displays endopeptidase activity. *Journal of Molecular Biology* 368: 509-520

Lamesch P, Berardini TZ, Li D, Swarbreck D, Wilks C, Sasidharan R, et al. (2012) The Arabidopsis Information Resource (TAIR): improved gene annotation and new tools. *Nucleic Acids Research* 40: D1202-D1210

Lang EGE, Mueller SJ, Hoernstein SNW, Porankiewicz-Asplund J, Vervliet-Scheebaum M, Reski R (2011) Simultaneous isolation of pure and intact chloroplasts and mitochondria from moss as the basis for sub-cellular proteomics. *Plant Cell Reports* 30: 205–215

Lang D, Ullrich KK, Murat F, Fuchs J, Jenkins J, Haas FB, et al. (2018) The *Physcomitrella patens* chromosome-scale assembly reveals moss genome structure and evolution. *Plant Journal* 93: 515-533

Laufs P, Peaucelle A, Morin H, Traas J (2004) MicroRNA regulation of the CUC genes is required for boundary size control in Arabidopsis meristems. *Development* 131: 4311-4322

Lee JH, Ryu HS, Chung KS, Posé D, Kim S, Schmid M, Ahn JH (2013) Regulation of temperature-responsive flowering by MADS-box transcription factor repressors. *Science* 342: 628-632

Lee KC, Chung KS, Lee HT, Park JH, Lee JH, Kim JK (2020) Role of Arabidopsis splicing factor SF1 in temperature-responsive alternative splicing of FLM pre-mRNA. *Frontiers in Plant Science* 11: 1917

Levey S, Wingler A (2005) Natural variation in the regulation of leaf senescence and relation to other traits in Arabidopsis. *Plant, Cell & Environment* 28: 223-231

Lingner T, Kataya AR, Antonicelli GE, Benichou A, Nilssen K, Chen XY, et al. (2011) Identification of novel plant peroxisomal targeting signals by a combination of machine learning methods and *in vivo* subcellular targeting analyses. *Plant Cell* 23: 1556-1572

López-Otín C, Blasco MA, Partridge L, Serrano M, Kroemer G (2013) The hallmarks of aging. *Cell* 153: 1194-1217

Lorenz S, Tintelnot S, Reski R, Decker EL (2003) Cyclin D-knockout uncouples developmental progression from sugar availability. *Plant Molecular Biology* 53: 227-236

Mao C, Zhu Y, Cheng H, Yan H, Zhao L, Tang J, et al. (2018) Nitric oxide regulates seedling growth and mitochondrial responses in aged oat seeds. *International Journal of Molecular Sciences* 19: 1052

Marshall I, Prince D, Johnson H, Ruiz D, Nicholaou M, Covey TM (2019) Analyzing the activity and expression of acyl peptide enzyme hydrolase (APEH) in the blood serum of patients with type II diabetes. *Bios* 90: 70-78

Maxwell DP, Wang Y, McIntosh L (1999) The alternative oxidase lowers mitochondrial reactive oxygen production in plant cells. *Proceedings of the National Academy of Sciences U.S.A.* 96: 8271-8276

Medina R, Johnson MG, Liu Y, Wickett NJ, Shaw J, Goffinet B (2019) Phylogenomic delineation of *Physcomitrium* (Bryophyta: Funariaceae) based on targeted sequencing of nuclear exons and their flanking regions rejects the retention of *Physcomitrella*, *Physcomitridium* and *Aphanorrhegma*. *Journal of Systematics and Evolution* 57: 404-417

Merchant SS, Prochnik SE, Vallon O, Harris EH, Karpowicz SJ, Witman GB, et al. (2007) The *Chlamydomonas* genome reveals the evolution of key animal and plant functions. *Science* 318: 245-250

Mergner J, Frejno M, List M, Papacek M, Chen X, Chaudhary A, et al. (2020) Mass-spectrometry-based draft of the *Arabidopsis* proteome. *Nature* 579: 409-414

Menyhárd DK, Kiss-Szemán A, Tichy-Rács É, Hornung B, Rádi K, Szeltner Z, et al. (2013) A self-compartmentalizing hexamer serine protease from *Pyrococcus horikoshii*: substrate selection achieved through multimerization. *Journal of Biological Chemistry* 288: 17884-17894

Mistry J, Chuguransky S, Williams L, Qureshi M, Salazar GA, Sonnhammer EL, et al. (2021) Pfam: The protein families database in 2021. *Nucleic Acids Research* 49: D412-D419

Mittler R, Zandalinas SI, Fichman Y, Van Breusegem F (2022) Reactive oxygen species signalling in plant stress responses. *Nature Reviews Molecular Cell Biology*: https://doi.org/10.1038/s41580-022-00499-2

Mogk A, Bukau B, Kampinga HH (2018) Cellular handling of protein aggregates by disaggregation machines. *Molecular Cell* 69: 214-226

Møller IM (2001) Plant mitochondria and oxidative stress: electron transport, NADPH turnover, and metabolism of reactive oxygen species. *Annual Review of Plant Biology* 52: 561-591

Møller IM, Jensen PE, Hansson A (2007) Oxidative modifications to cellular components in plants. *Annual Review of Plant Biology* 58: 459-481

Mueller SJ, Lang D, Hoernstein SNW, Lang EGE, Schuessele C, Schmidt A, et al. (2014) Quantitative analysis of the mitochondrial and plastid proteomes of the moss *Physcomitrella patens* reveals protein macrocompartmentation and microcompartmentation. *Plant Physiology* 164: 2081-2095

Müller-Schüssele SJ, Wang R, Gütle DD, Romer J, Rodriguez-Franco M, Scholz M, et al. (2020) Chloroplasts require glutathione reductase to balance reactive oxygen species and maintain efficient photosynthesis. *Plant Journal* 103: 1140-1154

Munné-Bosch S, Alegre L (2002) Plant aging increases oxidative stress in chloroplasts. *Planta* 214: 608-615

Nakai A, Yamauchi Y, Sumi S, Tanaka K. (2012) Role of acylamino acid-releasing enzyme/oxidized protein hydrolase in sustaining homeostasis of the cytoplasmic antioxidative system. *Planta* 236: 427–436

Nguyen ND, Mirarab S, Kumar K, Warnor T (2015) Ultra-large alignments using phylogeny-aware profiles. *Genome Biology* 16: 124

Noctor G, Veljovic-Jovanovic S, Driscoll S, Novitskaya L, Foyer CH (2002) Drought and oxidative load in the leaves of C3 plants: a predominant role for photorespiration? *Annals of Botany* 89: 841-850

Noy-Malka C, Yaari R, Itzhaki R, Mosquna A, Gershovitz NA, Katz A, Ohad N (2014) A single CMT methyltransferase homolog is involved in CHG DNA methylation and development of *Physcomitrella patens*. *Plant Molecular Biology* 84: 719-735

Orr MW, Mao Y, Storz G, Qian SB (2020) Alternative ORFs and small ORFs: shedding light on the dark proteome. *Nucleic Acids Research* 48: 1029-1042

Ostendorf AK, van Gessel N, Malkowsky Y, Sabovljevic MS, Rensing SA, Roth-Nebelsick A, Reski R (2021) Polyploidization within the Funariaceae – a key principle behind speciation, sporophyte reduction and the high variance of spore diameters? *Bryophyte Diversity and Evolution* 43: 164-179

Ouyang S, Zhu W, Hamilton J, Lin H, Campbell M, Childs K, et al. (2007) The TIGR rice genome annotation resource: improvements and new features. *Nucleic Acids Research* 35: D883-D887

Özdemir B, Asgharzadeh P, Birkhold AI, Mueller SJ, Röhrle O, Reski R (2018) Cytological analysis and structural quantification of FtsZ1-2 and FtsZ2-1 network characteristics in *Physcomitrella patens*. *Scientific Reports* 8: 11165

Palmieri G, Bergamo P, Luini A, Ruvo M, Gogliettino M, Langella E, et al. (2011) Acylpeptide hydrolase inhibition as targeted strategy to induce proteasomal down-regulation. *PLOS ONE* 6: e25888

Palmieri G, Cocca E, Gogliettino M, Valentino R, Ruvo M, Cristofano G, et al. (2017) Low erythrocyte levels of proteasome and acyl-peptide hydrolase (APEH) activities in Alzheimer's disease: a sign of defective proteostasis? *Journal of Alzheimer's Disease* 60: 1097-1106

Palumbo R, Gogliettino M, Cocca E, Iannitti R, Sandomenico A, Ruvo M, et al. (2016) APEH inhibition affects osteosarcoma cell viability via downregulation of the proteasome. *International Journal of Molecular Sciences* 17: 1614

Paradis E, Schliep K (2018) ape 5.0: an environment for modern phylogenetics and evolutionary analyses in R. *Bioinformatics* 35: 526-528

Parsell DA, Kowal AS, Singer MA, Lindquist S (1994) Protein disaggregation mediated by heat-shock protein Hspl04. *Nature* 372: 475-478

Perez-Riverol, Y, Bai, J, Bandla, C, García-Seisdedos, D, Hewapathirana, S, Kamatchinathan, S, et al. (2022). The PRIDE database resources in 2022: a hub for mass spectrometry-based proteomics evidences. *Nucleic Acids Research* 50: D543-D552

Perroud PF, Haas FB, Hiss M, Ullrich KK, Alboresi A, Amirebrahimi M, et al. (2018) The *Physcomitrella patens* gene atlas project: large-scale RNA-seq based expression data. *Plant Journal* 95: 168-182

Petriv, I, Tang, L, Titorenko, VI, Rachubinski, RA (2004). A new definition for the consensus sequence of the peroxisome targeting signal type 2. *Journal of Molecular Biology* 341: 119-134

Polgar L (2002) The prolyl oligopeptidase family. *Cellular and Molecular Life Sciences* 59: 349-362

Posé D, Verhage L, Ott F, Yant L, Mathieu J, Angenent GC, et al. (2013) Temperature-dependent regulation of flowering by antagonistic FLM variants. *Nature* 503: 414-417

Queitsch C, Hong SW, Vierling E, Lindquist S (2000) Heat shock protein 101 plays a crucial role in thermotolerance in Arabidopsis. *Plant Cell* 12: 479-492

R Core Team (2022) R: A language and environment for statistical computing. R Foundation for Statistical Computing, Vienna, Austria. URL https://www.R-project.org/.

Rankenberg T, Geldhof B, van Veen H, Holsteens K, van de Poel B, Sasidharan R (2021) Age-dependent abiotic stress resilience in plants. *Trends in Plant Science* 26: 692-705

Ratajczak E, Małecka A, Ciereszko I, Staszak AM (2019) Mitochondria are important determinants of the aging of seeds. *International Journal of Molecular Sciences* 20: 1568

Rawlings ND, Polgar L, Barrett AJ (1991) A new family of serine-type peptidases related to prolyl oligopeptidase. *Biochemical Journal* 279: 907-908

Rawlings ND, Barrett AJ, Thomas PD, Huang X, Bateman A, Finn RD (2018) The MEROPS database of proteolytic enzymes, their substrates and inhibitors in 2017 and a comparison with peptidases in the PANTHER database. *Nucleic Acids Research* 46: D624-D632

Reski R, Abel WO (1985) Induction of budding on chloronemata and caulonemata of the moss, *Physcomitrella patens*, using isopentenyladenine. *Planta* 165: 354-358

Reumann, S (2004) Specification of the peroxisome targeting signals type 1 and type 2 of plant peroxisomes by bioinformatics analyses. *Plant Physiology* 135: 783-800

Reumann S, Buchwald D, Lingner T (2012) PredPlantPTS1: a web server for the prediction of plant peroxisomal proteins. *Frontiers in Plant Science* 3: 194

Riccio A, Gogliettino M, Palmieri G, Balestrieri M, Facchiano A, Rossi M, et al. (2015) A new APEH cluster with antioxidant functions in the antarctic hemoglobinless icefish *Chionodraco hamatus*. *PLOS ONE* 10: e0125594

Rugen N, Schaarschmidt F, Eirich J, Finkemeier I, Braun HP, Eubel H (2021) Protein interaction patterns in *Arabidopsis thaliana* leaf mitochondria change in dependence to light. *Biochimica et Biophysica Acta (BBA)-Bioenergetics* 1862: 148443.

Sambrook J, Russell DW (2006) Standard ethanol precipitation of DNA in microcentrifuge tubes. *Cold Spring Harbor Protocols* 2006: pdb-prot4456

Scaloni A, Jones W, Pospischil M, Sassa S, Schneewind O, Popowicz AM, et al. (1992) Deficiency of acylpeptide hydrolase in small-cell lung carcinoma cell lines. *Journal of Laboratory and Clinical Medicine* 120: 546-552

Schuessele C, Hoernstein SNW, Mueller SJ, Rodriguez-Franco M, Lorenz T, Lang D, Igloi G, Reski R (2016) Spatio-temporal patterning of arginyl-tRNA protein transferase (ATE) contributes to gametophytic development in a moss. *New Phytologist* 209: 1014–1027

Schween G, Hohe A, Koprivova A, Reski R (2003) Effects of nutrients, cell density and culture techniques on protoplast regeneration and early protonema development in a moss, *Physcomitrella patens*. *Journal of Plant Physiology* 160: 209–212

Senthilkumar R, Reddy PN, Sharma KK (2001) Studies on trypsin-modified bovine and human lens acylpeptide hydrolase. *Experimental Eye Research* 72: 301-310

Sharma P, Jha AB, Dubey RS, Pessarakli M (2012) Reactive oxygen species, oxidative damage, and antioxidative defense mechanism in plants under stressful conditions. *Journal of Botany* 2012: 217037

Shimizu K, Fujino T, Ando K, Hayakawa M, Yasuda H, Kikugawa K (2003) Overexpression of oxidized protein hydrolase protects COS-7 cells from oxidative stress-induced inhibition of cell growth and survival. *Biochemical and Biophysical Research Communications* 304: 766-771

Shimizu K, Kiuchi Y, Ando K, Hayakawa M, Kikugawa K (2004) Coordination of oxidized protein hydrolase and the proteasome in the clearance of cytotoxic denatured proteins. *Biochemical and Biophysical Research Communications* 324: 140–146

Singh A, Singh S, Panigrahi KCS, Reski R, Sarkar AK (2014) Balanced activity of microRNA166/165 and its target transcripts from the class III homeodomain-leucine zipper family regulates root growth in *Arabidopsis thaliana*. *Plant Cell Reports* 33: 945-953

Smakowska E, Czarna M, Janska H (2014) Mitochondrial ATP-dependent proteases in protection against accumulation of carbonylated proteins. *Mitochondrion* 19: 245-251

Smirnoff N (2000) Ascorbic acid: metabolism and functions of a multi-facetted molecule. *Current Opinion in Plant Biology* 3: 229-235

Soares C, Carvalho ME, Azevedo RA, Fidalgo F (2019) Plants facing oxidative challenges—A little help from the antioxidant networks. *Environmental and Experimental Botany* 161: 4-25

Sohal RS & Weindruch R (1996) Oxidative stress, caloric restriction, and aging. *Science*, 273: 59-63.

Sperschneider J, Catanzariti AM, DeBoer K, Petre B, Gardiner DM, Singh KB, et al. (2017) LOCALIZER: subcellular localization prediction of both plant and effector proteins in the plant cell. *Scientific Reports* 7: 44598

Stamatakis A (2014) RAxML version 8: a tool for phylogenetic analysis and post-analysis of large phylogenies. *Bioinformatics* 30: 1312–1313

Suyama M, Torrents D, Bork P (2006) PAL2NAL: robust conversion of protein sequence alignments into the corresponding codon alignments. *Nucleic Acids Research* 34: W609–W612

Sweetlove LJ, Heazlewood JL, Herald V, Holtzapffel R, Day DA, Leaver CJ, Millar AH (2002) The impact of oxidative stress on Arabidopsis mitochondria. *Plant Journal* 32: 891-904

Szeltner Z, Kiss AL, Domokos K, Harmat V, Náray-Szabó G, Polgár L (2009) Characterization of a novel acylaminoacyl peptidase with hexameric structure and endopeptidase activity. *Biochimica et Biophysica Acta (BBA)-Proteins and Proteomics* 1794: 1204-1210

Tangri A, Lighty K, Loganathan J, Mesmar F, Podicheti R, Zhang C, et al. (2021) Deubiquitinase UCHL1 maintains protein homeostasis through the PSMA7–APEH–Proteasome axis in high-grade serous ovarian carcinoma. *Molecular Cancer Research* 19: 1168-1181

Tian GW, Mohanty A, Chary SN, Li S, Paap B, Drakakaki G, et al. (2004) High-throughput fluorescent tagging of full-length *Arabidopsis* gene products in planta. *Plant Physiology* 135: 25-38

Tiwari BS, Belenghi B, Levine A (2002) Oxidative stress increased respiration and generation of reactive oxygen species, resulting in ATP depletion, opening of mitochondrial permeability transition, and programmed cell death. *Plant Physiology* 128: 1271-1281

Tola AJ, Jaballi A, Missihoun TD (2021) Protein carbonylation: Emerging roles in plant redox biology and future prospects. *Plants* 10: 1451

Top O, Milferstaedt SW, van Gessel N, Hoernstein SNW, Özdemir B, Decker EL, Reski R (2021) Expression of a human cDNA in moss results in spliced mRNAs and fragmentary protein isoforms. *Communications Biology* 4: 964

Tsunasawa S, Narita K, Ogata K (1975) Purification and properties of acylamino acid-releasing enzyme from rat liver. *Journal of Biochemistry* 77: 89-102

Tuskan GA, DiFazio S, Jansson S, Bohlmann J, Grigoriev I, Hellsten U, et al. (2006) The genome of black cottonwood, *Populus trichocarpa* (Torr. & Gray). *Science* 313: 1596-1604

Tyanova S, Temu T, Sinitcyn P, Carlson A, Hein MY, Geiger T, et al. (2016) The Perseus computational platform for comprehensive analysis of (prote)omics data. *Nature Methods* 13: 731-740

van Wijk KJ, Leppert T, Sun Q, Boguraev SS, Sun Z, Mendoza L, Deutsch EW (2021) The Arabidopsis PeptideAtlas: Harnessing worldwide proteomics data to create a comprehensive community proteomics resource. *Plant Cell* 33: 3421-3453

Varshavsky A (2019) N-degron and C-degron pathways of protein degradation. *Proceedings of the National Academy of Sciences U.S.A.* 116: 358-366

Viaene T, Landberg K, Thelander M, Medvecka E, Pederson E, Feraru E, et al. (2014) Directional auxin transport mechanisms in early diverging land plants. *Current Biology* 24: 2786-2791

Wang J, Wang Y, Gao C, Jiang L, Guo D (2017) PPero, a computational model for plant PTS1 type peroxisomal protein prediction. *PLOS ONE* 12: e0168912

Wang QL, Chen JH, He NY, Guo FQ (2018) Metabolic reprogramming in chloroplasts under heat stress in plants. *International Journal of Molecular Sciences* 19: 849

Waszczak C, Carmody M, Kangasjärvi J (2018). Reactive oxygen species in plant signaling. *Annual Review of Plant Biology* 69: 209-236

Wei Q, Ma C, Xu Y, Wang T, Chen Y, Lü J, et al. (2017). Control of chrysanthemum flowering through integration with an aging pathway. *Nature Communications*, 8: 1-11

Weise A, Rodriguez-Franco M, Timm B, Hermann M, Link S, Jost W, Gorr G (2006) Use of *Physcomitrella patens* actin 5′ regions for high transgene expression: importance of 5′ introns. *Applied Microbiology and Biotechnology* 70: 337-345

Willems P, Ndah E, Jonckheere V, van Breusegem F, van Damme P (2021) To new beginnings: Riboproteogenomics discovery of N-terminal proteoforms in *Arabidopsis thaliana*. *Frontiers in Plant Science* 12: 778804

Wu G, Poethig RS (2006) Temporal regulation of shoot development in *Arabidopsis thaliana* by miR156 and its target SPL3. *Development* 131: 3539–3547

Yamauchi Y, Ejiri Y, Toyoda Y, Tanaka K (2003) Identification and biochemical characterization of plant acylamino acid–releasing enzyme. *Journal of Biochemistry* 134: 251-257

Yamin R, Zhao C, O'Connor PB, McKee AC, Abraham CR (2009) Acyl peptide hydrolase degrades monomeric and oligomeric amyloid-beta peptide. *Molecular Neurodegeneration* 4: 33

Yant L, Mathieu J, Dinh TT, Ott F, Lanz C, Wollmann H, et al. (2010) Orchestration of the floral transition and floral development in Arabidopsis by the bifunctional transcription factor APETALA2. *Plant Cell* 22: 2156-2170

Yu G, Smith D, Zhu H, Guan Y, Lam TT (2017) ggtree: an R package for visualization and annotation of phylogenetic trees with their covariates and other associated data. *Methods in Ecology and Evolution* 8: 28-36

Zeng Z, Rulten SL, Breslin C, Zlatanou A, Coulthard V, Caldecott KW (2017) Acylpeptide hydrolase is a component of the cellular response to DNA damage. *DNA Repair* 58: 52-61

Zhang H, Liu P, Guo T, Zhao H, Bensaddek D, Aebersold R, Xiong L (2019) Arabidopsis proteome and the mass spectral assay library. *Scientific Data* 6: 278

Zimmer AD, Lang D, Buchta K, Rombauts S, Nishiyama T, Hasebe M, et al. (2013) Reannotation and extended community resources for the genome of the non-seed plant *Physcomitrella patens* provide insights into the evolution of plant gene structures and functions. *BMC Genomics* 14: 498

Zybailov B, Rutschow H, Friso G, Rudella A, Emanuelsson O, Sun Q, van Wijk KJ (2008) Sorting signals, N-terminal modifications, and abundance of the chloroplast proteome. *PLOS ONE* 3: e1994

Supplemental Information

Figure S1 Expression levels of PpAARE genes and AtAARE in different tissues and under stress conditions

Figure S2 Sequence alignment of AtAARE and PtAARE isoforms.

Figure S3 AARE activity in Physcomitrella plastids and mitochondria.

Figure S4 Identification of PpAARE single, double and triple KO mutants by PCR on genomic DNA.

Figure S5 FCM analysis of all confirmed PpAARE KO lines to analyse the ploidy.

Figure S6 AARE exopeptidase activity protonema of KO mutants.

Figure S7 Plate overview and additional OxyBlots from Physcomitrella gametophore colonies with loading controls.

Figure S8 Screening for haploid Physcomitrella lines with a citrine fusion transcript and overview on identification of the three PpAARE isoforms in different IP experiments.

Figure S9 Phenotypes of seedlings and adult AtAARE T-DNA mutant lines (GK, s68) and WT (Col).

Table S1 List of primers used to assemble KO and KI constructs and primers used to screen for transgenic plants in Physcomitrella.

Table S2 List of gene accession numbers for all sequences used for phylogenetic analysis and corresponding subcellular localization predictions.

Table S3 List of primers used to screen possible T-DNA mutant plants in Arabidopsis.

Table S4 List of accession numbers for the International Moss Stock Center (IMSC) of all transgenic Physcomitrella lines.

Table S5 List of primers used for qPCR on genomic DNA to determine copy numbers of KO constructs in transgenic Physcomitrella lines.

Table S6 List of primers used to assemble the constructs for transient localization analysis in Physcomitrella protoplasts.

Table S7 This table contains the spectrum report of the revised database search of the anti-Arg$^{(Nt)}$ IP published in Hoernstein et al. (2016).

Supplemental figures

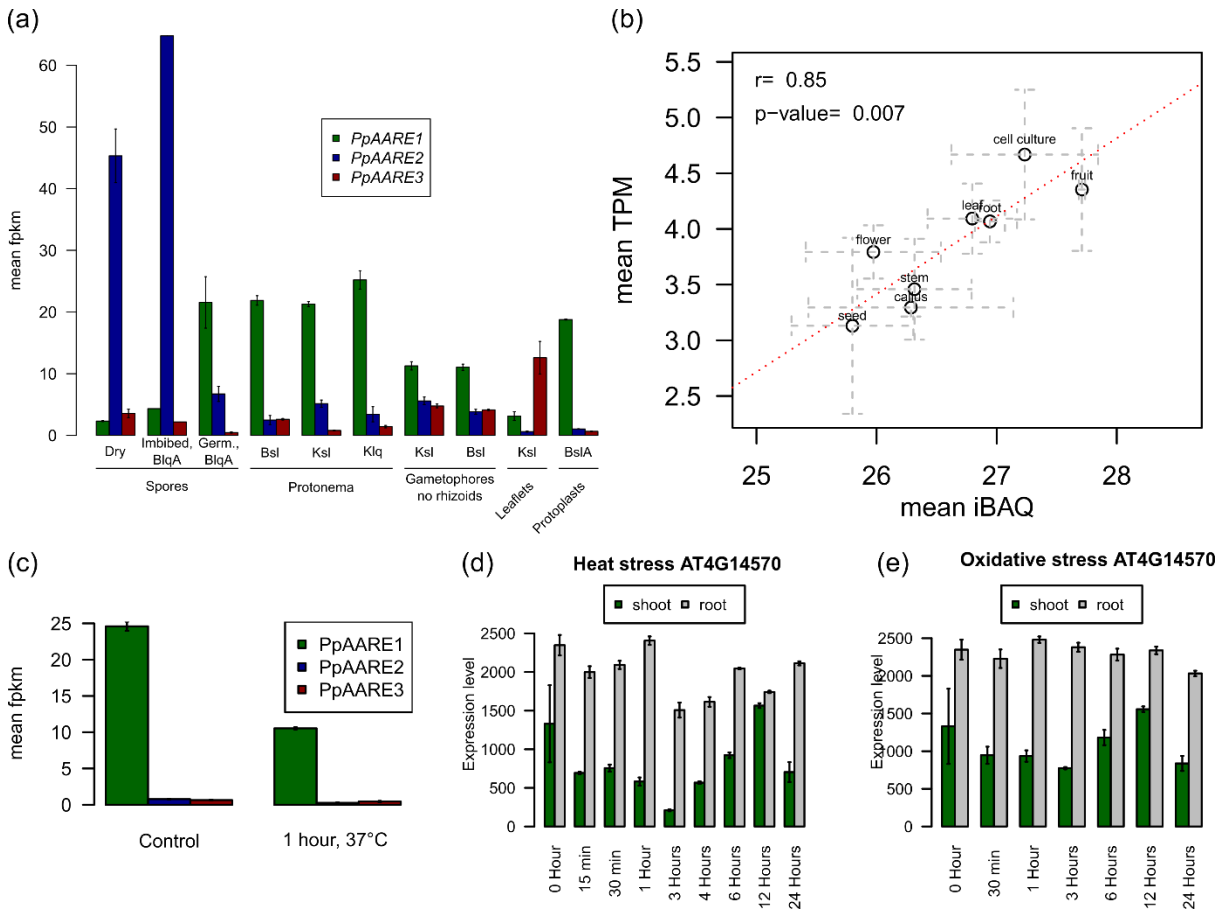

Fig. S1 Expression levels of PpAARE genes and AtAARE in different tissues and under stress conditions. (a) Expression levels of the three PpAARE isoforms in different tissue and cell culture types. Depicted are mean FPKM values with standard error (Perroud et al., 2018; Fernandez-Pozo et al., 2020). All data has been downloaded from *PEATmoss* (https://peatmoss.online.uni-marburg.de/). Abbreviations: B = BCD medium (Ashton et al., 1979); lq = liquid; A =ammonium tartrate; sl = solid; K = Knop medium; Germ. = germinating. (b) Tissue-specific expression levels of AtAARE and correlation between protein abundance and transcript level in Columbia WT (Col0). Transcript and protein abundance data have been downloaded from the *ATHENA* database (http://athena.proteomics.wzw.tum.de/) and were generated by Mergner et al. (2020). Transcript levels are represented by transcripts per million kilobase (TPM) and protein abundances are represented as intensity based absolute quantification values (iBAQ). Data points are mean values with standard deviation for each tissue group as obtained from *ATHENA*. Pearson´s correlation (r = 0.85) indicates a strong positive and significant (p-value = 0.007) correlation of expression levels and protein abundance in major tissue types. (c)

Expression levels for PpAARE1, PpAARE2 and PpAARE3 in Protonema in response to heat stress. Depicted are mean FPKM values with standard error. Data were downloaded from PEATmoss (https://peatmoss.online.uni-marburg.de/) and described in Perroud et al. (2018) and Fernandez-Pozo et al. (2020). (d) Expression levels of AtAARE in response to heat and oxidative stress (e). Data (d, e) were downloaded from the Arabidopsis eFP Browser (http://bar.utoronto.ca/efp_arabidopsis/) and described in Kilian et al. (2007) and Winter et al. (2007).

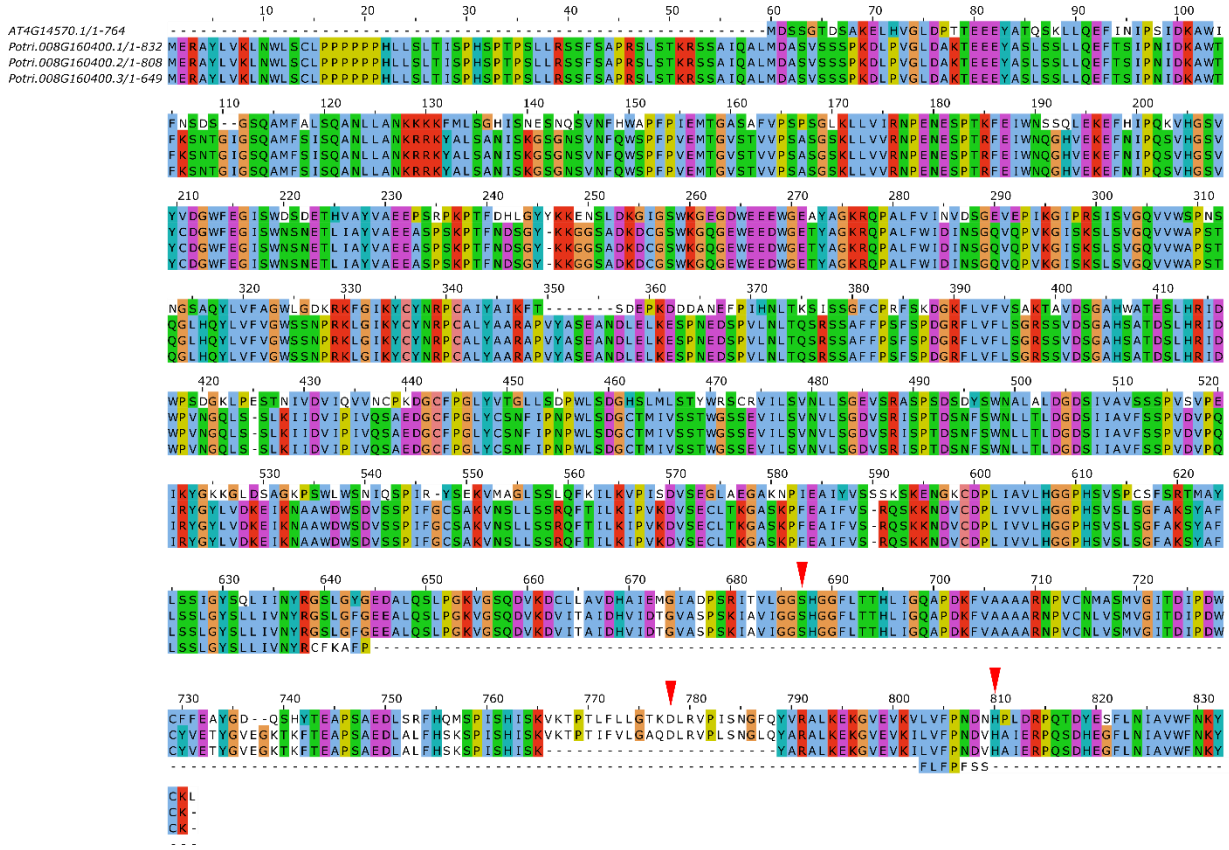

Fig. S2 Sequence alignment of AtAARE and PtAARE isoforms. Red arrows point to the catalytic residues (Ser, Asp, His) of AtAARE as described in Yamauchi et al. (2003). Two splice variants result in non-functional protein isoforms. Potri.008G160400.2 lacks the catalytic Asp (alignment position 778) and Potri.008G160400.3 is lacking the whole catalytic domain. Sequences were aligned in Jalview (Version: 2.11.1.3, Waterhouse et al., 2009) using T-Coffee (Notredame et al., 2000) with default settings.

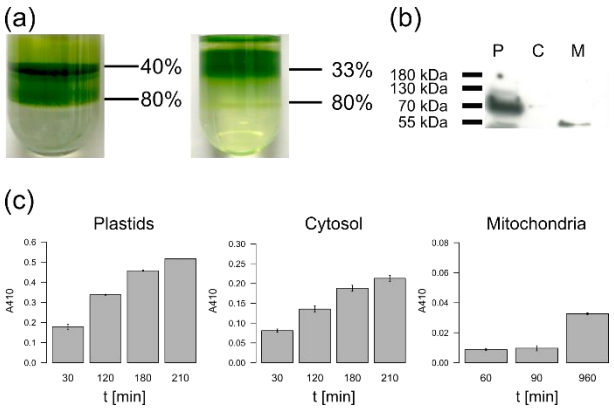

Fig. S3 AARE activity in Physcomitrella plastids and mitochondria. (a) Plastids and mitochondria were simultaneously isolated from the protonema as described in Lang et al. (2011). Intact plastids were collected at the interface between 80% and 40% Percoll, mitochondria were collected at the interface between 80% and 33% Percoll. (b) Cross-contamination of the obtained fractions with plastid proteins was assessed via Western Blot against the plastid HSP70B (Agrisera, AS06 175). Fractions were soluble plastid proteins (P), the soluble fraction depleted of plastids and mitochondria (referred to as cytosol, (C)) and soluble mitochondrial proteins (M). The intracellular and mitochondrial fraction was free of plastid cross-contaminations. (c) AARE activity measured using AcAla-pNA is present in isolated plastid fractions and in organelle-depleted intracellular fractions. Only low activity is detectable in mitochondrial fractions. The activity is indicated by the increase of the absorbance at 410 nm (A_{410}) over time caused by the release of pNA. Mean values from technical triplicates with standard deviation are shown.

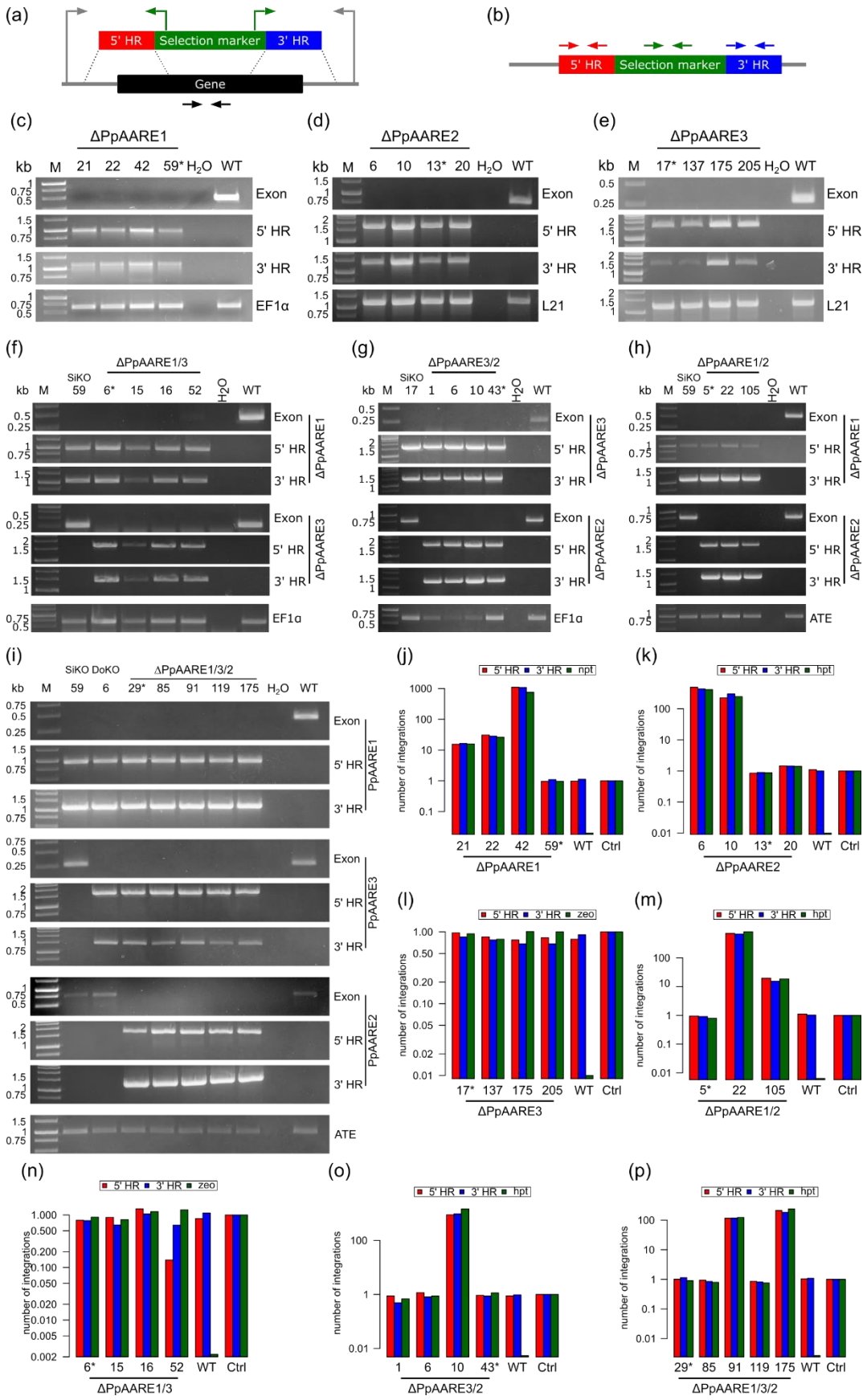
(a)
5' HR
Selection marker
3' HR
Gene
(b)
5' HR
Selection marker
3' HR
(c)
ΔPpAARE1
kb M 21 22 42 59* H2O WT
Exon
5' HR
3' HR
EF1α
(d)
ΔPpAARE2
kb M 6 10 13* 20 H2O WT
Exon
5' HR
3' HR
L21
(e)
ΔPpAARE3
kb M 17* 137 175 205 H2O WT
Exon
5' HR
3' HR
L21
(f)
ΔPpAARE1/3
SiKO
kb M 59 6* 15 16 52 H2O WT
Exon
5' HR
3' HR
ΔPpAARE1
ΔPpAARE3
EF1α
(g)
ΔPpAARE3/2
SiKO
kb M 17 1 6 10 43* H2O WT
ΔPpAARE3
ΔPpAARE2
EF1α
(h)
ΔPpAARE1/2
SiKO
kb M 59 5* 22 105 H2O WT
ΔPpAARE1
ΔPpAARE2
ATE
(i)
SiKO DoKO
ΔPpAARE1/3/2
kb M 59 6 29* 85 91 119 175 H2O WT
PpAARE1
PpAARE3
PpAARE2
ATE
(j)
5' HR 3' HR npt
number of integrations
21 22 42 59* WT Ctrl
ΔPpAARE1
(k)
5' HR 3' HR hpt
number of integrations
6 10 13* 20 WT Ctrl
ΔPpAARE2
(l)
5' HR 3' HR zeo
number of integrations
17* 137 175 205 WT Ctrl
ΔPpAARE3
(m)
5' HR 3' HR hpt
number of integrations
5* 22 105 WT Ctrl
ΔPpAARE1/2
(n)
5' HR 3' HR zeo
number of integrations
6* 15 16 52 WT Ctrl
ΔPpAARE1/3
(o)
5' HR 3' HR hpt
number of integrations
1 6 10 43* WT Ctrl
ΔPpAARE3/2
(p)
5' HR 3' HR hpt
number of integrations
29* 85 91 119 175 WT Ctrl
ΔPpAARE1/3/2

Fig. S4 Identification of PpAARE single, double and triple KO mutants by PCR on genomic DNA. (a) PCR scheme showing the primer combinations (arrows) used to validate KOs. One pair each is used to check for the correct positioning of the homologous flanks (5' and 3' HR) at the desired locus (green, gray) and one pair was used to check for the presence/absence of the genomic region (black arrows). (b) Scheme showing primers (arrows) used for qPCR on genomic DNA to determine the copy numbers of the KO construct integrated in the genome. Primers are listed in Table S2 and Table S5. Identification of single KOs for PpAARE1 (c), PpAARE2 (d) and PpAARE3 (e). Identification of ∆PpAARE1/3 (f), ∆PpAARE3/2 (g), ∆PpAARE1/2 (h) double KO lines and ∆PpAARE1/3/2 triple KO lines (i). SiKO indicate the single KO line employed as parental line for the generation of a double KO. ∆PpAARE1/3 #6 was employed as parental line for the generation of ∆PpAARE1/3/2 triple KO lines. Expected amplicon sizes for PpAARE1 KO PCR: Exon: 497 bp; 5' HR: 983 bp; 3' HR: 1128 bp. Expected amplicon sizes for PpAARE2 KO PCR: Exon: 768 bp; 5' HR: 1678 bp; 3' HR: 1309 bp. Expected amplicon sizes for PpAARE3 KO PCR: Exon: 273 bp; 5' HR: 1631 bp; 3' HR: 1486 bp. EF1α, L21 and ATE are reference genes (Table S2). Expected amplicon sizes: EF1α: 660 bp; L21: 1173 bp; 970 bp. (j)-(p) Copy number count of the respective KO constructs for each validated KO line determined via qPCR. Ctrl: Single copy integration control for each employed selection marker. Stars indicate lines with only a single genomic integration of the KO construct selected for further experiments.

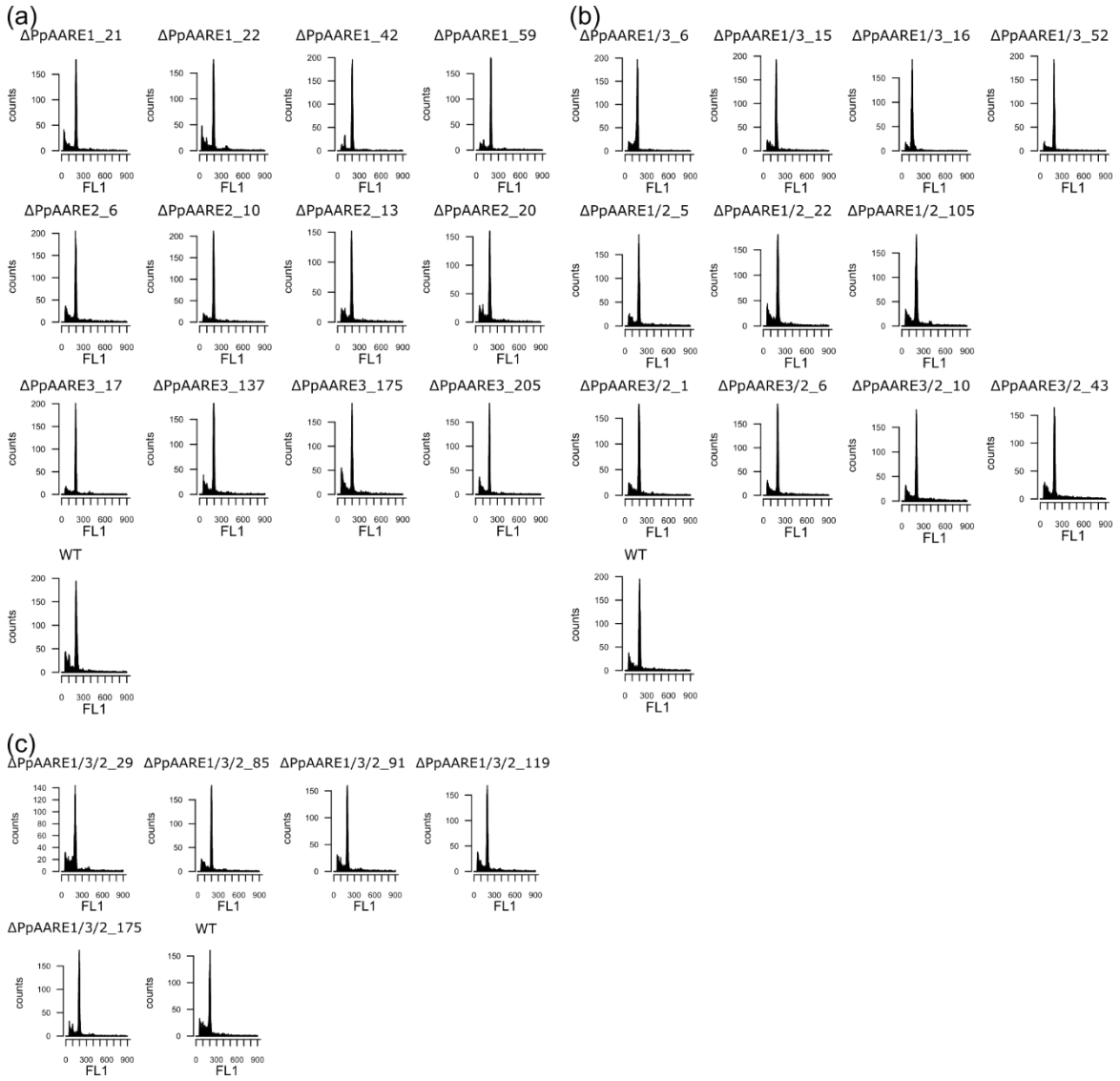

Fig. S5 FCM analysis of all confirmed PpAARE KO lines to analyse the ploidy. (a) Single KO lines, (b) double KO Lines, (c) triple KO lines. All lines have the major signal at ~200 like the haploid wild type. Ploidy was determined in protonema as described in Heck et al. (2021).

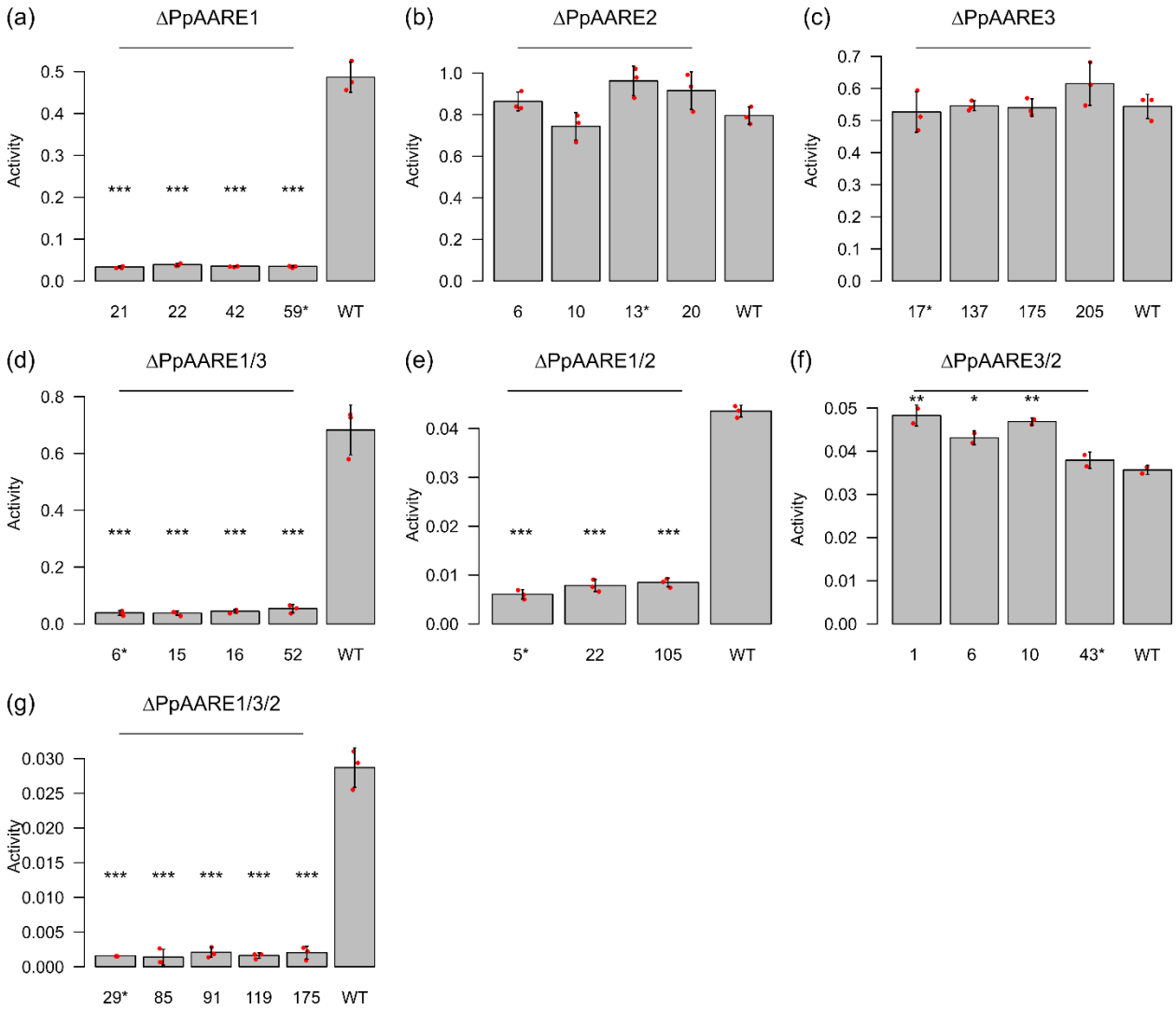

Fig. S6 AARE exopeptidase activity in protonema of KO mutants. AcAla-pNA was used as substrate and activity. Depicted is the mean activity of three technical replicates with standard deviation. Means of activity in ΔPpAARE3/2 lines are based on technical duplicates. Significance levels are based on a one-way Anova with subsequent post-hoc test (*: $p<0.05$, **: $p>0.01$, ***: $p<0.001$) and indicate differences compared to the wild type (WT). All lines with a knockout of PpAARE1 have significantly reduced activity (a, d, e, and g). (b). The mean activity is not reduced in ΔPpAARE2 and ΔPpAARE3 lines (c). The double knockout of ΔPpAARE3/2 (f) results in a significantly increase of activity in lines #1, #6, #10. Stars at the line numbers indicate the lines with only a single copy of the respective knockout construct which were used for the major experiments in this study.

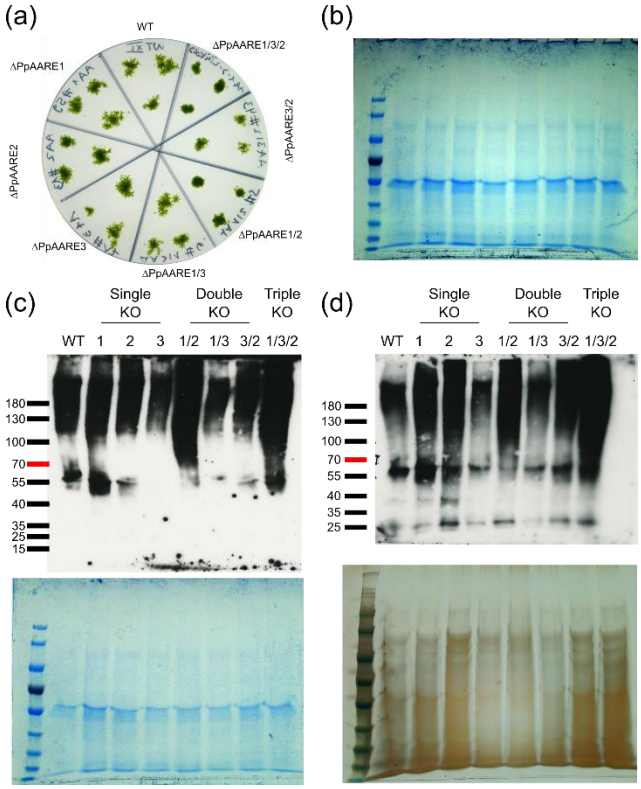

Fig. S7 Plate overview and additional OxyBlots from Physcomitrella gametophore colonies with loading controls. (a) Exemplary plate (KnopME) with five-week-old gametophore colonies from WT, single, double and triple knockouts. Protein extracts from single colonies were used for OxyBlot analysis. (b) Coomassie-stained loading control for the OxyBlot depicted in Fig. 3. (c+d) Additional OxyBlots with Coomassie- (c) and silver-stained (d) loading controls. Equal volumes from the same derivatized protein solutions were loaded for the OxyBlot as well as for the loading control gels. PageRuler™ Pre-stained Protein Ladder (Thermo Scientific™, #26166) was used for all Blots and loading control gels. OxyBlot analysis was performed with the OxyBlot™ *Protein Oxidation Detection Kit* (Merck) according to the manufacturer's instructions.

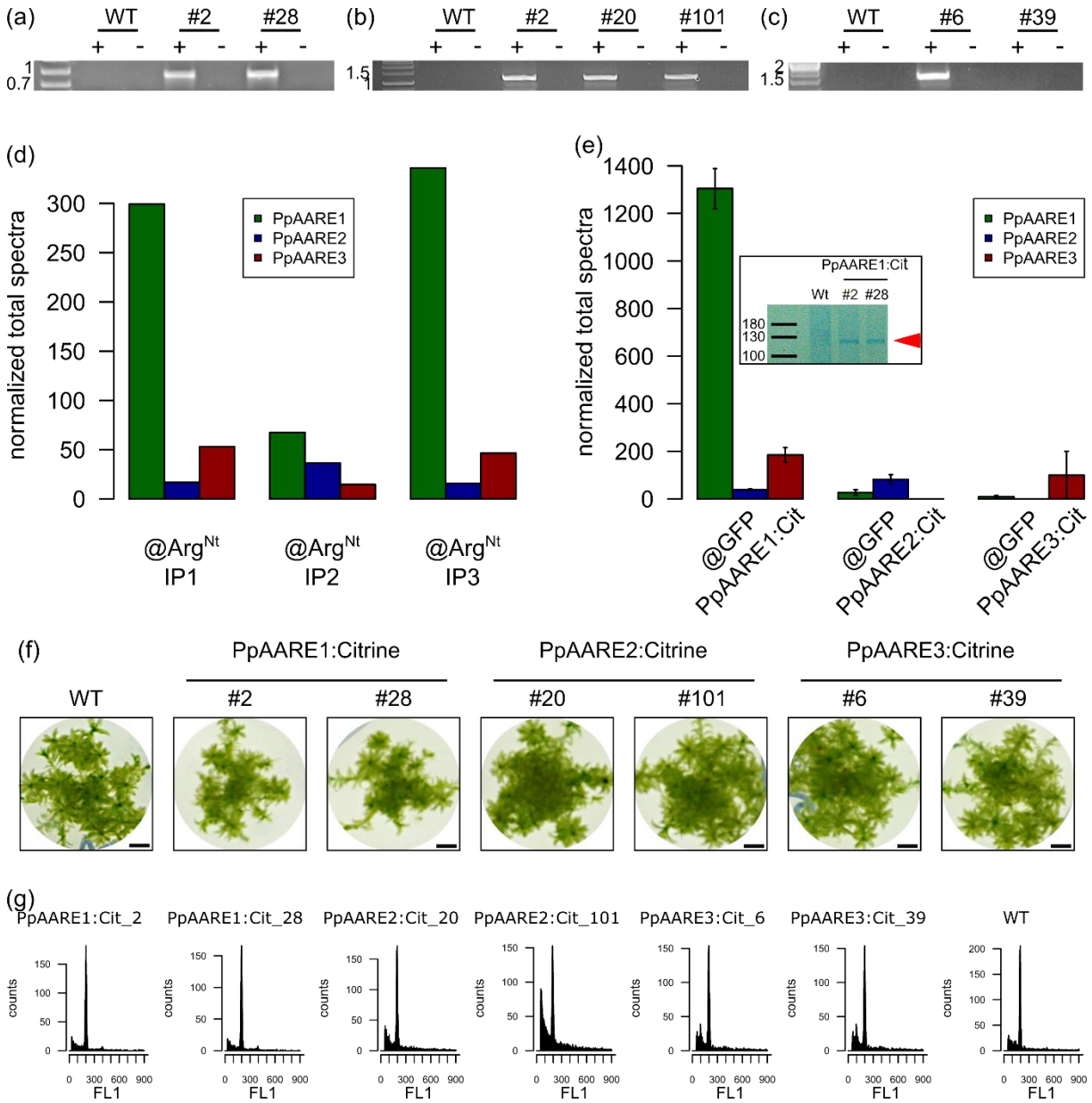

Fig. S8 Screening for haploid Physcomitrella lines with a citrine fusion transcript and overview on identification of the three PpAARE isoforms in different IP experiments. (a)-(c): RT PCR on citrine fusion candidate lines for PpAARE1 (a), PpAARE2 (b), and PpAARE3 (c). +: with cDNA template; -: without reverse transcriptase. For each PCR a forward primer binding in the CDS of the respective PpAARE isoform and a reverse primer binding in the CDS of citrine was chosen. Primers are listed in Table S2. No transcript was detected in PpAARE3:Citrine #6. PpAARE2:Citrine #2 was not used for further experiments. (d) All PpAARE isoforms were identified in the IP experiments targeting N-terminal arginylation (Hoernstein et al., 2016).

Identified proteins are listed in Table S7. (e) Overview on identification of PpAARE isoforms in the test IP experiments targeting the citrine tag of the different fusion proteins. The test IP against PpAARE1:Citrine was performed using *Dynabeeds M270 Epoxy Co-Immunoprecipitation Kit* (Life Technologies, Carlsbad, USA) with a monoclonal anti-GFP antibody (Roche, REF 11 814 460 001) as described in for two independent fusion lines (#2 and #28). Eluted proteins were separated via SDS-PAGE and bands (inset, red arrow) corresponding to the expected size (112 kDa) were excised and analysed by mass spectrometry. Test IP experiments against citrine-tagged PpAARE2 and PpAARE3 were performed with GFP-Trap Magnetic Particles (Chromotek) followed by an on-bead digestion with trypsin and subsequent mass spectrometry. Bars represent mean values with standard deviation of normalized total spectra obtained in each two independent fusion lines (PpAAR2: #20, #101; PpAARE3: #6, #39). (f) Gametophore colonies of selected Citrine fusion lines cultivated 4 months on solid medium. Bar = 2 mm. (g) FCM analysis of all confirmed PpAARE citrine fusion lines. Ploidy was determined in protonema as described in Heck et al. (2021). All lines have the major signal at ~200 like the haploid wild type.

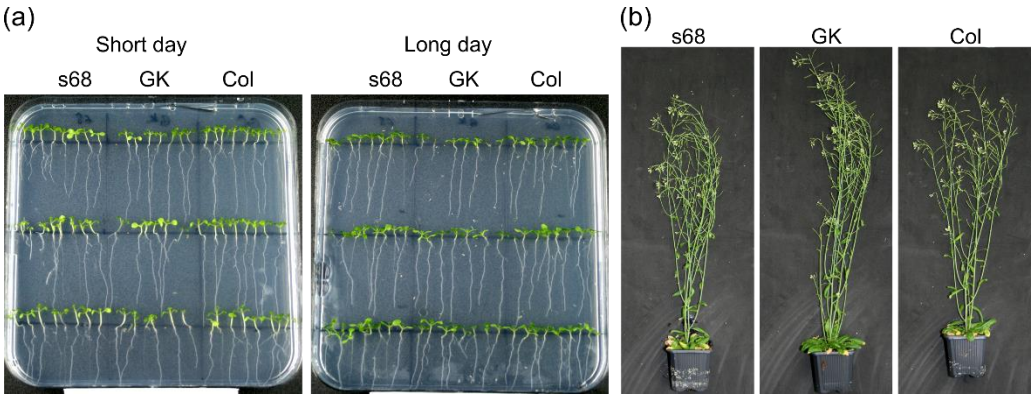

Fig. S9 Phenotypes of seedlings and adult AtAARE T-DNA mutant lines (GK, s68) and WT (Col). (a) AtAARE T-DNA mutant lines and WT germinated in short- or long-day conditions. Short day: 8h light /16h dark, 35 µmol/m^2s; Long day: 16h light / 8h dark, 35 µmol/m^{-2}s. (b) Adult plants cultivated for 7 weeks. Plants were grown under short day conditions (8h light/16h dark) for 4 weeks and then transferred to long day conditions for another 3 weeks (16h light/8h dark).

Supplemental References

Fernandez-Pozo N, Haas FB, Meyberg R, Ullrich KK, Hiss M, Perroud PF, et al. (2020) PEATmoss (Physcomitrella Expression Atlas Tool): a unified gene expression atlas for the model plant *Physcomitrella patens*. *Plant Journal* 102: 165-177

Heck MA, Lüth VM, van Gessel N, Krebs M, Kohl M, Prager A, Joosten H, Decker EL, Reski R (2021) Axenic *in vitro* cultivation of 19 peat moss (*Sphagnum* L.) species as a resource for basic biology, biotechnology, and paludiculture. *New Phytologist* 229: 861-876

Hoernstein SNW, Mueller SJ, Fiedler K, Schuelke M, Vanselow JT, Schuessele C, et al. (2016) Identification of targets and interaction partners of arginyl-tRNA protein transferase in the moss *Physcomitrella patens*. *Molecular & Cellular Proteomics* 15: 1808-1822

Kilian J, Whitehead D, Horak J, Wanke D, Weinl S, Batistic O, et al. (2007) The AtGenExpress global stress expression data set: protocols, evaluation and model data analysis of UV-B light, drought and cold stress responses. *Plant Journal* 50: 347-363

Notredame C, Higgins DG, Heringa J (2000) T-Coffee: A novel method for fast and accurate multiple sequence alignment. *Journal of Molecular Biology* 302: 205-217

Perroud PF, Haas FB, Hiss M, Ullrich KK, Alboresi A, Amirebrahimi M, et al. (2018) The *Physcomitrella patens* gene atlas project: large-scale RNA-seq based expression data. *Plant Journal* 95: 168-182

Waterhouse AM, Procter JB, Martin DM, Clamp M, Barton GJ (2009) Jalview Version 2—a multiple sequence alignment editor and analysis workbench. *Bioinformatics* 25: 1189-1191

Winter D, Vinegar B, Nahal H, Ammar R, Wilson GV, Provart NJ (2007) An “Electronic Fluorescent Pictograph” browser for exploring and analyzing large-scale biological data sets. *PLOS ONE* 2: e718

Yamauchi Y, Ejiri Y, Toyoda Y, Tanaka K (2003) Identification and biochemical characterization of plant acylamino acid–releasing enzyme. *Journal of Biochemistry* 134: 251-257

Mergner J, Frejno M, List M, Papacek M, Chen X, Chaudhary A, et al. (2020) Mass-spectrometry-based draft of the *Arabidopsis* proteome. *Nature* 579: 409-414